

Nonlinear Model Order Reduction of Dynamical Systems in Process Engineering: Review and Comparison

Jan C. Schulze^a and Alexander Mitsos^{b,a,c,*}

^a Process Systems Engineering (AVT.SVT), RWTH Aachen University, 52074 Aachen, Germany

^b JARA-CSD, 52056 Aachen, Germany

^c Energy Systems Engineering (ICE-1), Forschungszentrum Jülich, 52425 Jülich, Germany

Abstract. Computationally cheap yet accurate enough dynamical models are vital for real-time capable nonlinear optimization and model-based control. When given a computationally expensive high-order prediction model, a reduction to a lower-order simplified model can enable such real-time applications. Herein, we review state-of-the-art nonlinear model order reduction methods and provide a theoretical comparison of method properties. Additionally, we discuss both general-purpose methods and tailored approaches for (chemical) process systems and we identify similarities and differences between these methods. As manifold-Galerkin approaches currently do not account for inputs in the construction of the reduced state subspace, we extend these methods to dynamical systems with inputs. In a comparative case study, we apply eight established model order reduction methods to an air separation process model: POD-Galerkin, nonlinear-POD-Galerkin, manifold-Galerkin, dynamic mode decomposition, Koopman theory, manifold learning with latent predictor, compartment modeling, and model aggregation. Herein, we do not investigate hyperreduction (reduction of FLOPS). Based on our findings, we discuss strengths and weaknesses of the model order reduction methods.

Keywords: model simplification, hybrid model, invariant manifold, nonlinear Galerkin, machine learning

1. Introduction

Process systems in chemical engineering are inherently nonlinear, e.g., as a result of reaction kinetics, transport phenomena, and thermodynamic relationships [1]. Over the past decades, detailed mechanistic process modeling has become increasingly common in (chemical) process systems engineering (PSE). In particular, mechanistic first-principles models, accounting for conservation of mass, energy, and (less often) momentum, along with constitutive relations, possess favorable generalization capabilities. Hence, “digital twins” and “digital shadows” have been established as a valuable tool for process monitoring and operator training [2, 3]. However, in such predictive models, the high number of nonlinear differential equations is usually computationally prohibitive for online optimization and model-based control methods such as nonlinear model predictive control (NMPC). Furthermore, process models are often stiff, making them even more challenging to handle [4].

Model reduction is a popular technique to reduce the computational cost of optimization by means of model simplification. In this context, a reduction in the number of differential states is called “model order reduction” (MOR) and the resulting model is a “reduced-order model” (ROM) [5, 6]. Conversely, the original model is the “full-order model” (FOM). MOR is particularly used for spatially distributed systems, which are commonly described by partial differential equations or modeled as networks of lumped systems. Examples of high-order systems in PSE include computational fluid dynamics [7], distillation columns [8], heat exchangers [9], chemical reactors [10], and integrated process networks [11]. Fine-grained mechanistic modeling of such systems can result in thousands or millions of states.

Although mechanistic models can be very high-dimensional, FOMs often exhibit a certain coherence characterized by a few dominant mechanisms or patterns, e.g., due to stiffness of the system [12].

*Corresponding author: amitsos@alum.mit.edu

Provided that a part of the transients vanish after a short period of time due to dissipative phenomena with a comparably fast exponential decay, we obtain a time-scale separation between fast stable decay and slow response [13]. As a result, the high-dimensional state evolves most of the time near a low-dimensional topological subspace, referred to as “slow manifold”, “inertial manifold”, or “invariant manifold” [14, 15]. An accurate ROM is obtained when finding a low-order approximation of the FOM on the slow manifold. Such reducible systems are also called “lumpable” [16].

MOR methods construct low-order approximations of a FOM, i.e., a ROM, either by projecting the FOM onto the slow manifold [17, 18] or by identifying an empirical ROM directly from state data [19]. Projecting the FOM onto a linear subspace is called a “Galerkin projection” [20], a concept of high significance for this article. In many cases, a considerable reduction (removing 80 % of the states or more) of a FOM is possible at a minor sacrifice of accuracy. However, the range of validity of a ROM is considerably reduced as well, e.g., highly transient situations, such as process startup or shutdown, are usually no longer covered.

Reduction methods can be classified according to how the FOM is utilized [21]. Specifically, “intrusive methods” rely on structural and parametric knowledge of the FOM. A large subclass of intrusive methods are reduced-basis methods, which seek a low-dimensional set of basis vectors spanning a linear or affine subspace on which the system approximately evolves, followed by an (intrusive) projection of the FOM onto this subspace [22, 23]. Non-projection-based intrusive methods include simplifying assumptions and heuristic reduction. On the other hand, “non-intrusive methods” are fully detached from the FOM equations, i.e., model-free. These methods only require state time series data to generate a ROM.

Many projection-based approaches follow a two-stage procedure to derive a ROM. First, the nonlinear system is reversibly transformed into a favorable representation, e.g., some canonical or normal form. Subsequently, reduction is performed on the transformed system by systematic truncation or residualization of dynamic components. Depending on the original model and the reduction method, the resulting ROM can be anything from a white-box (all equations/terms have a physical meaning) to an almost black-box (purely empirical) model. Examples of the first step include proper orthogonal decomposition [24], input-output balancing [25, 26], singular perturbation canonical form [27], Weierstrass canonical form [28], canonical bilinear or polynomial form [29, 30, 31], and Koopman lifting [32, 33].

For some types of systems, e.g., convection-dominated systems, wave-type equations, and conservation problems, the assumption of a low-dimensional linear subspace does not hold [34]. Such systems live on a nonlinear submanifold rather than on a linear subspace [35]. Consequently, Galerkin projection requires a large number of basis vectors to retain high ROM accuracy [17, 36]. Instead, nonlinear subspace methods can approximate the nonlinear slow manifold more closely. Projecting the FOM onto the nonlinear submanifold is a “nonlinear Galerkin” [35] or “manifold-Galerkin” [36] projection. Fig. 1 illustrates the advantage of a nonlinear manifold. The state data generated by a 3D FOM approximately lie on a 2D linear (affine) or a 1D nonlinear subspace.

When reducing a nonlinear FOM, the CPU cost of evaluating a ROM is often not significantly decreased, despite the lower differential order [22]. Thus, to achieve a reduction in computational costs, an additional consecutive “hyperreduction” step is performed [37, 38], which reduces the arithmetic complexity (FLOPS). Hyperreduction is achieved by applying supervised approximation techniques to replace expensive terms by, e.g., piecewise linear functions [39, 40], polynomials [41, 42, 43], sparse regression models [44], or artificial neural networks (ANNs) [45, 37]. In some cases, semi-empirical shortcut methods are an alternative to eliminate steady-state equations of a ROM [46]. Further, hyperreduction methods may also be implemented in an adaptive fashion [47, 48]. In case of a differential-algebraic ROM, hyperreduction automatically eliminates algebraic equations, so a prior reduction of algebraic variables [49, 50] is often not required. Combining data-driven and mechanistic

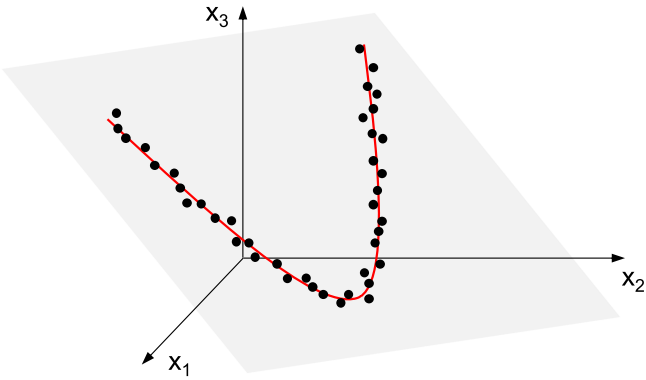


Fig. 1: Linear (■) vs. nonlinear (---) submanifold compared to FOM data points (●).

elements, the resulting ROM can be considered a “hybrid model”. Hyperreduction drives the ROM further towards a black-box model but is essential for real-time capability. The overall model reduction process thus typically involves the two ingredients (i) MOR and (ii) hyperreduction.

Although non-intrusive reduction methods do not operate on the FOM equations, these methods are still based on state information (and sometimes also on time derivative data). Conversely, the identification of a black-box model from input-output data does not involve any state data and thus lacks the information carried by the states. In particular, state information turn out to be highly valuable for many systems, where input-output system identification may struggle to extract sensible latent information [51].

Despite a long history of research, MOR remains an evolving field with major contributions made in recent years, e.g., [19, 52, 33, 36]. Comprehensive reviews of MOR are found in [53, 18, 7, 54, 55] as well as textbooks on linear [56, 20] and nonlinear MOR [57, 58, 59]. However, despite an extensive body of literature, available low-barrier introductory texts [5, 6] and comparative studies in the PSE field [60, 61, 7] lack a discussion of some recent developments. Furthermore, reduced modeling strategies that have been developed in the chemical engineering community are often not discussed in the general model reduction literature.

Over the years, managing the growing number of MOR options and making a suitable choice has become increasingly difficult. Therefore, this article aims to provide an overview of classical and more recent methods. We consider systems with inputs and focus on nonlinear state-space models, but we also include index-one differential-algebraic systems. We compare common methods both theoretically and in a PSE case study. As we target ROM application within NMPC and soft sensors, we want to preserve the knowledge of all states and retain flexibility in formulating the optimal control problem. Hence, we aim for ROMs that allow reconstruction of all original states and thus focus on input-to-state reduction methods rather than input-output methods. Consequently, we do not review input-output balancing methods for linear systems [25, 62], empirical extensions to nonlinear systems [63, 64, 26, 65], or data-driven moment matching [66]. Further, we disregard MOR methods based on linearized FOMs, e.g., applying feedback linearization before reduction [67].

The manuscript is structured as follows. First, we introduce a general version of the MOR problem for systems with inputs in Section 2. In Section 3, we provide an overview of general-purpose MOR methods. We divide this review into intrusive methods in Section 3.1 and non-intrusive methods in Section 3.2. During the review of intrusive methods, we observe that current manifold learning methods only involve the system states and do not account for external inputs (Section 3.1.4). Hence, we propose an extension in Section 3.1.5. The review of general-purpose methods concludes with a theoretical comparison in Section 3.3. In Section 4, we review problem-specific MOR approaches that have been developed in the field of PSE and draw connections to methods in Section 3. Additionally, we review applications of MOR for three important unit operations, namely distillation columns,

heat exchangers, and reactors. Section 5 provides a comparative case study, where we reduce the process model of an air separation unit (ASU). Therein, we compare eight MOR approaches that are selected as a representative ensemble of the methods reviewed. Notably, we limit ourselves to MOR and do not consider hyperreduction and CPU costs of integration to avoid an extra level of methods and complexity. However, we expect that any ROM of sufficiently low order can be made real-time capable by appropriate hyperreduction. In Section 6, we summarize and discuss the strengths and weaknesses of the MOR methods. Section 7 concludes the manuscript.

Notation. Given a matrix $\mathbf{A} \in \mathbb{R}^{n \times m}$, $\mathbf{A} = [\mathbf{a}_1, \dots, \mathbf{a}_m]$, the linear space spanned by the column vectors $\mathbf{a}_i \in \mathbb{R}^n$ is denoted by $\mathcal{A} = \text{col}(\mathbf{A})$ and called the “column space” of \mathbf{A} . Given a real non-square matrix \mathbf{A} , the “pseudoinverse” is $\mathbf{A}^+ \triangleq (\mathbf{A}^T \mathbf{A})^{-1} \mathbf{A}^T$. Given some domain \mathcal{X} , we denote by $\mathcal{C}^r(\mathcal{X})$ the set of r -times continuously differentiable functions over \mathcal{X} , $r \geq 1$, and call a function f smooth if $f \in \mathcal{C}^\infty(\mathcal{D})$. We denote the identity matrix by \mathbf{I} . Given a single independent coordinate $t \in \mathbb{R}$ (here time), we call the map $\gamma : \mathbb{R} \rightarrow \mathbb{R}^n$ a “curve”. We denote the velocity of a curve γ at time t by $\dot{\gamma}(t) \triangleq \frac{d\gamma}{dt}|_t$. Given some \mathcal{C}^r -map $\mathbf{f} : \mathbb{R}^n \rightarrow \mathbb{R}^m$ between Euclidean spaces \mathbb{R}^n and \mathbb{R}^m , where $n, m \geq 1$, we denote the linear “differential map” of \mathbf{f} at $\mathbf{x} \in \mathbb{R}^n$ by $D\mathbf{f} : \mathbb{R}^n \rightarrow \mathbb{R}^m$. Given some point $\mathbf{x} \in \mathbb{R}^n$, we associate $D\mathbf{f}$ with its Jacobian matrix $D\mathbf{f}(\mathbf{x}) \in \mathbb{R}^{m \times n}$. For a function $\mathbf{f}(\mathbf{x}, \mathbf{y})$ of two arguments, we consider $D_{\mathbf{x}}\mathbf{f}(\mathbf{x}, \mathbf{y})$ and $D_{\mathbf{y}}\mathbf{f}(\mathbf{x}, \mathbf{y})$ separately. An “immersion” is a smooth map, $\mathbf{h} : \mathcal{Z} \subseteq \mathbb{R}^{n_z} \rightarrow \mathcal{X} \subseteq \mathbb{R}^{n_x}$, satisfying $\text{rank}(D_z \mathbf{h}^\dagger(\cdot)) = n_z$ (injective) everywhere in \mathcal{Z} .

We consider embedded submanifolds of ambient space \mathbb{R}^n characterized in terms of level sets. The respective definition is intuitive and sufficiently general for our purposes.

Definition 1 (Level set, [68]). *Let $\mathbf{c} : \mathcal{X} \rightarrow \mathbb{R}^m$, $\mathcal{X} \subseteq \mathbb{R}^n$ open, $1 \leq m < n$, be a \mathcal{C}^r -mapping, $r \geq 1$. Denote by $\mathcal{M} \subseteq \mathbb{R}^n$ the zero level set:*

$$\mathcal{M} = \{\mathbf{x} \in \mathbb{R}^n : \mathbf{c}(\mathbf{x}) = \mathbf{0}\}. \quad (1)$$

Assume that \mathcal{M} is non-empty and the Jacobian $D\mathbf{c}(\mathbf{x}) \in \mathbb{R}^{m \times n}$ has constant rank m at all $\mathbf{x} \in \mathcal{M}$. Then, \mathcal{M} is a manifold of class \mathcal{C}^r , i.e., a differentiable manifold. Moreover, \mathcal{M} has dimension $k = n - m$ and is embedded in \mathbb{R}^n , and therefore called an “embedded k -submanifold” of \mathbb{R}^n . By the definition of continuity, the preimage $\mathcal{M} = \mathbf{c}^{-1}(\{\mathbf{0}\})$ is closed in \mathbb{R}^n and therefore \mathcal{M} is said to be properly embedded.

We remark that the embedding is not an essential part of the definition, i.e., there exist more generic definitions that are independent of an ambient space [68]. Therefore, we sometimes drop the terms “embedded” or “sub” (manifold). Note that \mathbb{R}^n is a manifold itself. By limiting ourselves to embedded submanifolds of (open subsets $\mathcal{X} \subseteq \mathbb{R}^n$ of) Euclidean space \mathbb{R}^n defined through level sets, we circumvent geometric concepts like charts and tangent bundles. We refer the interested reader to [68, 69, 70].

2. Model order reduction problem

In this section, we present a general formulation of the MOR problem. We are concerned with two types of non-autonomous dynamical systems. We focus on nonlinear dynamical systems with external inputs, described by a system of ordinary differential equations (ODE):

$$\dot{\mathbf{x}}(t) = \mathbf{f}(\mathbf{x}(t), \mathbf{u}(t)), \quad (2)$$

where $t \in [t_0, t_\infty]$ denotes time, $\mathbf{x}(t) \in \mathcal{X}$ denote the differential states, $\mathcal{X} \subseteq \mathbb{R}^{n_x}$, $\mathbf{u}(t) \in \mathcal{U}$, $\mathcal{U} \subseteq \mathbb{R}^{n_u}$, and $\mathbf{f} : \mathcal{X} \times \mathcal{U} \rightarrow \mathbb{R}^{n_x}$ smooth. We call \mathcal{X} the state space, \mathcal{U} the input space, and Eq. (2) a state space model. The dimension n_x is the “model order”. The model is “strictly causal”, because $\mathbf{x}(t)$ depends only on $\mathbf{u}(\tau)$, $\tau < t$, and thus $\dot{\mathbf{u}}(t)$ does not appear in Eq. (2).

We further allow semi-explicit differential-algebraic systems of equations (DAE) with external inputs:

$$\dot{\mathbf{x}}(t) = \mathbf{f}(\mathbf{x}(t), \mathbf{y}(t), \mathbf{u}(t)), \quad (3a)$$

$$\mathbf{0} = \mathbf{g}(\mathbf{x}(t), \mathbf{y}(t), \mathbf{u}(t)), \quad (3b)$$

where $\mathbf{x}(t) \in \mathcal{X} \subseteq \mathbb{R}^{n_x}$, $\mathbf{y}(t) \in \mathcal{Y} \subseteq \mathbb{R}^{n_y}$ are the algebraic variables, and $\mathbf{u}(t) \in \mathcal{U} \subseteq \mathbb{R}^{n_u}$ are the external inputs. Let \mathcal{X} , \mathcal{Y} and \mathcal{U} be open, and $\mathbf{f} : \mathcal{X} \times \mathcal{Y} \times \mathcal{U} \rightarrow \mathbb{R}^{n_x}$ and $\mathbf{g} : \mathcal{X} \times \mathcal{Y} \times \mathcal{U} \rightarrow \mathbb{R}^{n_y}$ be smooth. We say that the DAE has “index one” if $D_y \mathbf{g}(\hat{\mathbf{x}}, \hat{\mathbf{y}}, \hat{\mathbf{u}})$ has rank n_y for any $(\hat{\mathbf{x}}, \hat{\mathbf{u}}) \in \hat{\mathcal{X}} \times \hat{\mathcal{U}}$ on the solution set of \mathbf{g} [4, 71].

The class of semi-explicit DAEs covers a wide range of models within PSE, where ODEs are often not sufficiently versatile. However, MOR methods are typically developed for ODEs. Fortunately, this is not a problem because an index-one DAE (3) may be regarded as an ODE that lives on a submanifold of $\hat{\mathcal{X}} \times \hat{\mathcal{Y}} \times \hat{\mathcal{U}}$ [72, 15]. Applying definition 1 to Eq. (3b) verifies this claim. Moreover, higher-index DAEs can usually be reduced to index-one systems [4]. Consequently, we can adopt ODE methods to index-one DAEs [73, 47]. For conciseness, we will only consider FOMs of the form (2). However, the methods can also be applied to Eq. (3) under the assumption of index-one.

The second reason for introducing both Eqs. (2) and (3) is that some MOR methods reduce a high-order ODE to a low-order DAE, which we generally assume to be index-one. Hence, we will frequently encounter ROMs of the form Eq. (3). Next, we formalize the MOR problem for nonlinear systems with external inputs:

Problem 1 (MOR). *Given a FOM (2), find a low-order index-one DAE (the prototype of a ROM):*

$$\dot{\mathbf{z}}(t) = \mathbf{f}_r(\mathbf{z}(t), \mathbf{u}(t)), \quad (4a)$$

$$\mathbf{0} = \mathbf{h}(\mathbf{z}(t), \mathbf{x}_r(t), \mathbf{u}(t)), \quad (4b)$$

where differential states $\mathbf{z}(t) \in \mathcal{Z}$, $\mathcal{Z} \subseteq \mathbb{R}^{n_z}$, $n_z \ll n_x$, algebraic variables $\mathbf{x}_r(t) \in \mathcal{X}$ that approximate the FOM states $\mathbf{x}(t)$, and $\mathbf{f}_r : \mathcal{Z} \times \mathcal{U} \rightarrow \mathbb{R}^{n_z}$, and $\mathbf{h} : \mathcal{Z} \times \mathcal{X} \times \mathcal{U} \rightarrow \mathbb{R}^{n_x}$ are smooth. Let Eq. (4) be such that for any $\mathbf{x}(t_0) \in \mathcal{X}$ and any $\mathbf{u}(t) \in \mathcal{U}$, $t \geq t_0$, the prediction error $\|\mathbf{x}_r(t) - \mathbf{x}(t)\| < \varepsilon$ holds for all $t \geq t_0$ and $\varepsilon \geq 0$ sufficiently small.

We call Eq. (4a) the “latent dynamics” or “internal dynamics”. A suitable value of n_z depends on the FOM, the relevant time scales, and the desired ROM accuracy. For simplicity, we do not impose further requirements on the upper bound ε , e.g., existence of a contraction mapping.

Next, we characterize the subset(s) of \mathcal{X} on which the ROM (4) evolves. To this end, we examine the level set:

$$\mathcal{M} \triangleq \{(\hat{\mathbf{x}}, \hat{\mathbf{z}}, \hat{\mathbf{u}}) \in \mathcal{X} \times \mathcal{Z} \times \mathcal{U} : \mathbf{0} = \mathbf{h}(\hat{\mathbf{x}}, \hat{\mathbf{z}}, \hat{\mathbf{u}})\}. \quad (5)$$

According to definition 1, \mathcal{M} constitutes a smooth embedded submanifold of $\mathcal{X} \times \mathcal{Z} \times \mathcal{U}$, where $\dim \mathcal{M} = n_z + n_u$. In addition, when fixing $\mathbf{u}_0 \in \mathcal{U}$, the level set:

$$\mathcal{M}_{\mathcal{X}}(\mathbf{u}_0) = \{\hat{\mathbf{x}} \in \mathcal{X} : \mathbf{0} = \mathbf{h}(\hat{\mathbf{x}}, \hat{\mathbf{z}}, \mathbf{u}_0), \hat{\mathbf{z}} \in \mathcal{Z}\} \quad (6)$$

constitutes a smooth embedded n_z -submanifold of \mathcal{X} , where $\mathcal{M}_{\mathcal{X}}(\mathbf{u}_0) \times \{\mathbf{u}_0\}$ is a slice of \mathcal{M} . To satisfy the requirements in ?? 1, we search for an invariant manifold \mathcal{M} having the property that $\mathbf{f}(\mathbf{x}(t), \mathbf{u}(t))$ is tangent to $\mathcal{M}_{\mathcal{X}}(\mathbf{u}(t))$ if $\mathbf{x}(t) \in \mathcal{M}_{\mathcal{X}}(\mathbf{u}(t))$. Then, Eq. (4) solves the invariance equations (closure condition):

$$\forall (\hat{\mathbf{x}}, \hat{\mathbf{z}}, \hat{\mathbf{u}}) \in \mathcal{M} : D_x \mathbf{h}(\hat{\mathbf{x}}, \hat{\mathbf{z}}, \hat{\mathbf{u}}) \mathbf{f}(\hat{\mathbf{x}}, \hat{\mathbf{u}}) + D_z \mathbf{h}(\hat{\mathbf{x}}, \hat{\mathbf{z}}, \hat{\mathbf{u}}) \mathbf{f}_r(\hat{\mathbf{z}}, \hat{\mathbf{u}}) = \mathbf{0}, \quad (7)$$

where $D_x \mathbf{h}(\cdot)^{-1}$ exists due to the index-one assumption and we have used $D_x \mathbf{h}(\cdot)^{-1} D_u \mathbf{h}(\cdot) \equiv \mathbf{0}$, since \mathbf{f} cannot depend on $\dot{\mathbf{u}}(t)$ due to strict causality.

A fundamental difference to autonomous systems is that changes in $\mathbf{u}(t)$ can affect $\mathcal{M}_{\mathcal{X}}$. For example, changing $\mathbf{u}(t)$ may rotate or shift the respective embedded $\mathcal{M}_{\mathcal{X}}$. If $\mathbf{u}(t)$ is piecewise constant, then $\mathcal{M}_{\mathcal{X}}$ may change its shape abruptly at the input grid points. If $\mathbf{u}(t)$ is continuous, then $\mathcal{M}_{\mathcal{X}}$ may gradually deform over time. When changing $\mathbf{u}(t)$ from \mathbf{u}_0 to \mathbf{u}_1 at time t_1 , the prior $\mathbf{x}_r^- \triangleq \lim_{t \nearrow t_1} \mathbf{x}_r(t)$ may not be in $\mathcal{M}_{\mathcal{X}}(\mathbf{u}_1)$. This offset is immediately addressed by a projection of \mathbf{x}_r^- onto $\mathcal{M}_{\mathcal{X}}(\mathbf{u}_1)$, inherently defined by Eq. (4b). This projection corresponds to the fast-time-scale response of the system to

changes in $\mathbf{u}(t)$. However, depending on \mathbf{h} , the associated projection can introduce unwanted artifacts in the ROM response (see discussion in Section 3.1.2).

A common simplification of Eq. (4) is to use a one-to-one immersion $\mathbf{h}^\dagger : \mathcal{Z} \rightarrow \mathcal{X}$, so that $\mathcal{M}_\mathcal{X} = \{\mathbf{h}^\dagger(\mathbf{z}) : \mathbf{z} \in \mathcal{Z}\}$ and $\dot{\mathbf{x}}_r(t) \in \text{col}(\mathbf{D}\mathbf{h}^\dagger(\mathbf{z}(t)))$ on \mathcal{M} . In this case, we have $\mathcal{M} = \mathcal{M}_\mathcal{X} \times \mathcal{U}$ (trivial bundle) and Eq. (7) becomes:

$$\forall(\hat{\mathbf{x}}, \hat{\mathbf{z}}, \hat{\mathbf{u}}) \in \mathcal{M} : \mathbf{f}(\hat{\mathbf{x}}, \hat{\mathbf{u}}) - \mathbf{D}_z \mathbf{h}^\dagger(\hat{\mathbf{z}}) \mathbf{f}_r(\hat{\mathbf{z}}, \hat{\mathbf{u}}) = \mathbf{0}. \quad (8)$$

3. General-purpose reduction methods

We review state-of-the-art reduction methods that are applicable to a wide range of systems, rather than developed for a specific type of process model. Additionally, in Section 3.1.5, we develop an extension of the manifold-Galerkin method (reviewed in Section 3.1.4) to explicitly account for the dependence of the slow manifold on the inputs. For the sake of brevity, we omit equations as far as possible and rather focus on an abstract discussion.

3.1. Intrusive general-purpose methods

We begin with a review of intrusive MOR methods, which involve the FOM equations in the MOR procedure. First, we discuss two classical intrusive approaches: proper orthogonal decomposition (POD) and singular perturbation theory (SPT). Afterwards, we present more recent extensions using machine learning, specifically manifold learning methods.

While POD belongs to the class of linear subspace methods, SPT constructs a nonlinear subspace. Linear subspace methods are typically divided into methods based on singular values decomposition (SVD) and Krylov subspace methods [74]. Herein, we do not discuss Krylov subspace methods [75], which are major reduction techniques for linear systems, but their extension to nonlinear MIMO systems is not straightforward. We refer to [29, 52] for some works towards this goal. An extensive overview of MOR using Krylov subspace methods is given in [18].

3.1.1. POD-Galerkin method

The POD, also known as Karhunen-Loéve decomposition, is a method to extract a low-dimensional linear basis capturing the dominant behavior of a system [76]. Usually, the POD basis is determined through SVD of discrete state trajectory samples (“snapshots”) from simulation studies. Define the data matrix $\mathbf{D} \in \mathbb{R}^{n_x \times N}$, $N \geq n_x$, by stacking N snapshots $\mathbf{x}^{(k)}$, $k = 1, 2, \dots, N$. Compute the mean $\bar{\mathbf{x}} \in \mathbb{R}^{n_x}$ and form the zero-centered matrix $\mathbf{X} = [\mathbf{x}^{(1)} - \bar{\mathbf{x}}, \dots, \mathbf{x}^{(N)} - \bar{\mathbf{x}}]$. Then, SVD provides:

$$\mathbf{X} = \mathbf{U} \mathbf{\Sigma} \mathbf{V}^T, \quad (9)$$

where $\mathbf{\Sigma} \in \mathbb{R}^{n_x \times n_s}$ is a non-square diagonal matrix of ordered entries σ_i , which are the “singular values”. The orthogonal matrices $\mathbf{U} \in \mathbb{R}^{n_x \times n_x}$ and $\mathbf{V} \in \mathbb{R}^{N \times N}$ collect the corresponding left and right singular (column) vectors, respectively. The columns of \mathbf{U} are also called “principal components” of \mathbf{X} , since they are ordered by their relevance to represent the data \mathbf{X} . As opposed to the eigendecomposition of \mathbf{X} , the SVD is well-conditioned and stable [20]. However, SVD is sensitive to data scaling, so improper scaling can result in a poor ROM [76].

The “POD-Galerkin method” consists of two main steps. First, SVD provides the “POD modes” \mathbf{U} . Next, we specify the reduced order $n_z < n_x$ and subdivide $\mathbf{U} = [\mathbf{U}_1, \mathbf{U}_2]$, where $\mathbf{U}_1 \in \mathbb{R}^{n_x \times n_z}$. Because \mathbf{U}_1 carries the dominant POD modes, we may truncate the mode \mathbf{U}_2 and use the approximation:

$$\mathbf{x}^{(k)} - \bar{\mathbf{x}} \approx \mathbf{U}_1 \mathbf{z}^{(k)}, \quad k = 1, 2, \dots, N, \quad (10)$$

where $\mathbf{z}^{(k)} \in \mathbb{R}^{n_z}$ are lower-dimensional coordinates and $\bar{\mathbf{x}} \in \mathbb{R}^{n_x}$ is the mean used in the SVD above. Eq. (10) corresponds to the optimal (“proper”) approximation of the data \mathbf{X} in the 2-norm [77]. However, the optimality of \mathbf{U}_1 refers only to the data set and not to ROM prediction accuracy [22].

Next, the affine subspace, $\mathcal{M}_{\mathcal{X}} = \{\bar{\mathbf{x}} + \mathbf{v} : \mathbf{v} \in \text{col}(\mathbf{U}_1)\}$, is defined as the reduced state space. Using Eq. (10), we perform a Galerkin projection of the FOM (2) onto the basis \mathbf{U}_1 and obtain the ROM [22]:

$$\begin{aligned}\dot{\mathbf{z}}(t) &= \mathbf{U}_1^T \mathbf{f}(\mathbf{U}_1 \mathbf{z}(t) + \bar{\mathbf{x}}, \mathbf{u}(t)), \\ \mathbf{x}_r(t) &= \mathbf{U}_1 \mathbf{z}(t) + \bar{\mathbf{x}}.\end{aligned}\quad (11)$$

The POD is data-driven and therefore non-intrusive, but subsequent Galerkin projection is intrusive. Combining data-driven reduced basis and physics-based FOM, the nonlinear ROM (11) is a hybrid model. As the original map \mathbf{f} is still contained in ROM (11), an additional hyperreduction step may be required to enable real-time applications [41]. In particular, the matrix \mathbf{U}_1 is usually dense, so a sparse model \mathbf{f} may lose its sparsity.

Due to CPU costs of SVD, the POD-Galerkin method is limited to problems with a few thousand states [20]. For bigger problems, sequential “greedy” approaches are a cheaper option [78, 34]. These methods minimize the (worst case) ∞ -norm of the error between reduced basis and snapshots rather than the least squares error or 2-norm. The reduced basis is then generally non-orthogonal and a projection onto such a basis is a “Petrov-Galerkin projection” [20]. Often, ROMs based on POD and greedy search reach a similar accuracy [79].

3.1.2. Singular perturbation theory

Model reduction by SPT is a nonlinear subspace method based on time-scale separation of a FOM [80]. Assume that the FOM (2) is originally in “singular perturbation canonical form” [27]:

$$\dot{\mathbf{x}}_1(t) = \mathbf{f}_1(\mathbf{x}_1(t), \mathbf{x}_2(t), \mathbf{u}(t)), \quad (12a)$$

$$\varepsilon \dot{\mathbf{x}}_2(t) = \mathbf{f}_2(\mathbf{x}_1(t), \mathbf{x}_2(t), \mathbf{u}(t)), \quad (12b)$$

where $\varepsilon \ll 1$ and $\mathbf{x}_1(t) \in \mathbb{R}^{n_z}$ and $\mathbf{x}_2(t) \in \mathbb{R}^{n_x - n_z}$. Equations (12a) and (12b) collect the “slow” and “fast dynamics”, respectively. We assume that exponential stability of the fast dynamics holds uniformly.

The key idea of perturbation theory is that the system response does not change significantly when ε is perturbed to even smaller values. When setting $\varepsilon = 0$ in Eq. (12), the fast dynamics degenerate into quasi-stationary equations, yielding a ROM defined by:

$$\dot{\mathbf{x}}_1(t) = \mathbf{f}_1(\mathbf{x}_1(t), \mathbf{x}_2(t), \mathbf{u}(t)), \quad (13a)$$

$$\mathbf{0} = \mathbf{f}_2(\mathbf{x}_1(t), \mathbf{x}_2(t), \mathbf{u}(t)). \quad (13b)$$

Assuming that Eq. (13) is index-one, the corresponding slow manifold is given by:

$$\mathcal{M} = \{(\mathbf{x}_1, \mathbf{x}_2, \mathbf{u}) \in \mathbb{R}^{n_z} \times \mathbb{R}^{n_x - n_z} \times \mathbb{R}^{n_u} : \mathbf{f}_2(\mathbf{x}_1, \mathbf{x}_2, \mathbf{u}) = \mathbf{0}\}. \quad (14)$$

Typically, a process model is initially not in the form (12) and identifying the perturbation parameter ε is not obvious [11]. Often, we seek for a linear transformation, $\mathbf{x}(t) = \mathbf{T}_1 \mathbf{x}_1(t) + \mathbf{T}_2 \mathbf{x}_2(t)$. For chemical systems, \mathbf{T}_1 and \mathbf{T}_2 are sometimes determined based on a time scale assumption on energy and mass transport [81, 82]. More rigorous approaches search for a subset of \mathcal{X} or $\mathcal{X} \times \mathcal{U}$ whose defect of invariance is sufficiently small [27, 83, 84].

An important property of Eq. (13) is that the steady-state response remains exact. However, the degeneration of the fast dynamics occasionally introduces undesirable dynamic artifacts, especially a non-physical inverse response (IR) [85, 86]. The appearance of an IR depends on the degree of reduction and the choice of \mathbf{T}_1 and \mathbf{T}_2 [87]. In control, a sign-reversed model gain can degrade the closed-loop behavior of NMPC toward infeasibility or instability. However, a false IR is only problematic when appearing on the prediction time grid of the ROM application, e.g., NMPC, where an extremely fast IR may be uncritical.

3.1.3. Redisualization method

Closely related to the singular perturbation method is the “POD residualization” (POD-Res) or “nonlinear-POD-Galerkin” method [88, 13]. Instead of Galerkin projection onto a linear subspace

via POD truncation, a nonlinear subspace ROM is obtained by considering the limit of infinitely fast (degenerate or “slaved”) dynamics. Let the POD modes $\mathbf{U} = [\mathbf{U}_1, \mathbf{U}_2, \mathbf{U}_3]$ so that $\mathbf{U}_1 \in \mathbb{R}^{n_x \times n_z}$ and $\mathbf{U}_2 \in \mathbb{R}^{n_x \times n_q}$, where $1 < n_q \leq n_x - n_z$. Accordingly, we first extend Eq. (11) to:

$$\dot{\mathbf{z}}_1(t) = \mathbf{U}_1^T \mathbf{f}(\mathbf{U}_1 \mathbf{z}_1(t) + \mathbf{U}_2 \mathbf{z}_2(t) + \bar{\mathbf{x}}, \mathbf{u}(t)) \quad (15a)$$

$$\dot{\mathbf{z}}_2(t) = \mathbf{U}_2^T \mathbf{f}(\mathbf{U}_1 \mathbf{z}_1(t) + \mathbf{U}_2 \mathbf{z}_2(t) + \bar{\mathbf{x}}, \mathbf{u}(t)), \quad (15b)$$

$$\mathbf{x}_r(t) = \mathbf{U}_1 \mathbf{z}_1(t) + \mathbf{U}_2 \mathbf{z}_2(t) + \bar{\mathbf{x}}. \quad (15c)$$

Then, by residualization of Eq. (15b), i.e., setting $\dot{\mathbf{z}}_2(t) = \mathbf{0}$, we obtain [17]:

$$\dot{\mathbf{z}}_1(t) = \mathbf{U}_1^T \mathbf{f}(\mathbf{U}_1 \mathbf{z}_1(t) + \mathbf{U}_2 \mathbf{z}_2(t) + \bar{\mathbf{x}}, \mathbf{u}(t)), \quad (16a)$$

$$\mathbf{0} = \mathbf{U}_2^T \mathbf{f}(\mathbf{U}_1 \mathbf{z}_1(t) + \mathbf{U}_2 \mathbf{z}_2(t) + \bar{\mathbf{x}}, \mathbf{u}(t)), \quad (16b)$$

$$\mathbf{x}_r(t) = \mathbf{U}_1 \mathbf{z}_1(t) + \mathbf{U}_2 \mathbf{z}_2(t) + \bar{\mathbf{x}}. \quad (16c)$$

Despite the POD-based partitioning of states in the first step, the residualization provides a *nonlinear* subspace due to Eq. (16b). In [60], the authors compared POD-Galerkin and POD-Res, finding that low-order POD-Res ROMs are more accurate than POD-Galerkin ROMs but also more computationally expensive without hyperreduction.

When setting $n_q = n_x - n_z$, i.e., applying an exhaustive residualization with no truncation, POD-Res can be regarded as an SPT method. This interpretation implies that the POD-based affine transformation divides the states into fast and slow dynamics. In our experience, a certain degree of POD truncation is possible without a relevant loss of precision, yet enabling a significant improvement of numerical conditioning. Therefore, we use $n_q < n_x - n_z$ below. Finally, there exist alternatives to POD in the context of nonlinear Galerkin methods [89, 35], e.g., using wavelets [90]. In the next subsection, we discuss another nonlinear Galerkin variant based on machine learning, which circumvents the residualization step and is fully detached from a linear POD basis.

3.1.4. Manifold-Galerkin method

Applying machine learning (ML) to approximate a manifold from snapshot data is called “manifold learning” (MFL) or “representation learning” [91]. MFL encompasses a wide array of tools and techniques that can be grouped into (i) ANN approaches, including autoencoder networks (AENs) [92, 93] and self-organizing maps [94], (ii) spectral methods, such as classical PCA or kernel PCA [95, 96], locally linear embeddings [97], Laplacian eigenmaps [98], and diffusion maps [99], and (iii) probabilistic methods [100]. These methods can also be combined, e.g., AENs and classical PCA [101].

Not all MFL methods are suitable for MOR via Galerkin projection. The subset of viable options includes AENs, self-organizing maps, and kernel PCA [36]. Herein, we focus on MOR using AENs. In particular, the simultaneous strength and weakness of AENs is their feedforward structure, which renders AENs conceptually and numerically simple to deal with. However, although AENs can be successfully applied in many cases, some manifolds cannot be globally represented by a single parameterization as provided by an AEN.

The structure of an AEN is illustrated by Fig. 2. We here consider “undercomplete” AENs, where $n_z < n_x$. First, the “encoder” network $\phi : \mathcal{X} \rightarrow \mathbb{R}^{n_z}$, $\mathcal{X} \subseteq \mathbb{R}^{n_x}$ open, projects the high-dimensional input vector $\mathbf{x} \in \mathcal{X}$ to a lower-dimensional representation $\mathbf{z} \in \mathbb{R}^{n_z}$. Often, \mathbf{z} are called “features” or “latent variables”. In the second step, the “decoder” network $\phi^\dagger : \mathcal{Z} \rightarrow \mathbb{R}^{n_x}$, where $\mathcal{Z} \subseteq \mathbb{R}^{n_z}$, reconstructs the high-dimensional vector from the features. The images of the two mappings are $\phi(\mathcal{X}) \subseteq \mathcal{Z}$ and $\phi^\dagger(\mathcal{Z}) \subseteq \mathcal{X}$. The standard unsupervised AEN training problem minimizes the mean squared reconstruction error (MSE), $\sum_{k=1}^N \|\mathbf{x}^{(k)} - \phi^\dagger \circ \phi(\mathbf{x}^{(k)})\|_2^2$, given a data set $\mathcal{D} = \{\mathbf{x}^{(k)}\}_{k=1}^N$ [102]. Assuming that ϕ^\dagger is a one-to-one immersion, the subset $\mathcal{M}_{\mathcal{X}} \triangleq \{\phi^\dagger(\hat{\mathbf{z}}) : \hat{\mathbf{z}} \in \mathcal{Z}\}$ is an n_z -dimensional embedded submanifold of \mathcal{X} . When using an MSE training loss, the composition $\phi^\dagger \circ \phi$ approximates an orthogonal projection from \mathcal{X} to $\mathcal{M}_{\mathcal{X}}$.

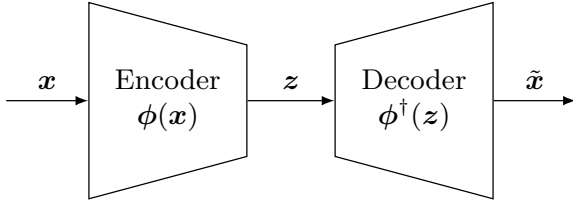


Fig. 2: Illustration of an autoencoder network.

Intrusive MOR based on AENs is presented in [103, 36] and refined in [101, 104]. Here, we adopt the method of [36] and we comment on the refinements below. Training an AEN on snapshots approximates the slow manifold by $\mathcal{M}_\mathcal{X}$. Differentiation of the approximation $\mathbf{x}(t) \approx \phi^\dagger(\mathbf{z}(t))$ and insertion into Eq. (2) yields:

$$\begin{aligned} D\phi^\dagger(\mathbf{z}(t))\dot{\mathbf{z}}(t) &= \mathbf{f}(\phi^\dagger(\mathbf{z}(t)), \mathbf{u}(t)), \\ \mathbf{x}_r(t) &= \phi^\dagger(\mathbf{z}(t)), \end{aligned} \quad (17)$$

where $\dot{\mathbf{z}}(t) \in \mathbb{R}^{n_z}$ and $\mathbf{x}_r(t) \in \mathbb{R}^{n_x}$. Clearly, the map ϕ^\dagger (and thus the activation function) need to be differentiable. To obtain a well-posed ROM, we multiply Eq. (17) by $D\phi^\dagger(\mathbf{z}(t))^\text{T}$:

$$D\phi^\dagger(\mathbf{z}(t))^\text{T} D\phi^\dagger(\mathbf{z}(t))\dot{\mathbf{z}}(t) = D\phi^\dagger(\mathbf{z}(t))^\text{T} \mathbf{f}(\phi^\dagger(\mathbf{z}(t)), \mathbf{u}(t)), \quad (18a)$$

$$\mathbf{x}_r(t) = \phi^\dagger(\mathbf{z}(t)). \quad (18b)$$

As a result, we obtain a ‘‘manifold-Galerkin’’ projection of FOM (2) onto $\mathcal{M}_\mathcal{X}$ [36]. By applying the definition of the pseudoinverse, $D\phi^\dagger(\mathbf{z}(t))^\dagger$, Eq. (18) can be finally brought into the form of Eq. (4):

$$\dot{\mathbf{z}}(t) = D\phi^\dagger(\mathbf{z}(t))^\dagger \mathbf{f}(\phi^\dagger(\mathbf{z}(t)), \mathbf{u}(t)), \quad (19a)$$

$$\mathbf{0} = \mathbf{x}_r(t) - \phi^\dagger(\mathbf{z}(t)). \quad (19b)$$

Note that Eq. (19) does not involve the encoding ϕ . While $\phi^\dagger(\mathbf{z}(t))$ is an embedding of \mathcal{Z} into \mathcal{X} , the map $D\phi^\dagger(\mathbf{z}(t))^\dagger$ is a linear projection from \mathbb{R}^{n_x} to \mathbb{R}^{n_z} (more precisely from the tangent space to \mathcal{X} at $\phi^\dagger(\mathbf{z}(t))$ onto the tangent space to \mathcal{Z} at $\mathbf{z}(t)$). When using a linear AEN, then Eq. (19) reduces to Eq. (11). In practice, we employ Eq. (18) rather than Eq. (19) to circumvent matrix inversion or SVD associated with pseudoinversion in the model. To improve ROM accuracy, the standard AEN training problem may be extended by an additional velocity loss [104]. We regard such an approach as a step towards ‘‘physics-informed’’ model reduction.

There exist alternative options to using manifold-Galerkin projection and the pseudoinverse. One alternative approach, that is also suitable when applying non-orthogonal (oblique) projections [104], is to apply the left-inverse property, $D\phi(\phi^\dagger(\mathbf{z})) \circ D\phi^\dagger(\mathbf{z}) = \mathbf{I}$, to Eq. (17). However, within preliminary studies, we found that this approach is sensitive to projection errors and therefore requires an advanced AEN training strategy.

The manifold-Galerkin projection using AENs increases the number of FLOPS considerably due to the added decoder network and its Jacobian. On the positive side, the slow manifold is represented by a feedforward ANN rather than by a set of implicit equations. For spatially distributed systems, computational improvements can be achieved by using convolutional instead of fully connected AENs [105, 106].

We are particularly interested in systems with input. Although [103, 36, 104] consider input-affine or parametric systems, these works do not account for the effect of inputs or parameters on the slow manifold, cf. Eq. (6). Instead, a trivial bundle $\mathcal{M} = \mathcal{M}_\mathcal{X} \times \mathcal{U}$ is constructed. However, we expect this simplification to demand an unnecessarily high-dimensional slow manifold. Consequently, we employ the concepts from Section 2 to propose a respective extension below.

3.1.5. Manifold-Galerkin method with inputs

We extend the manifold-Galerkin method [36] to account for the effect of system inputs on the slow manifold \mathcal{M} . Restricting ourselves to AENs, we are generally interested in maps of the form φ :

$\mathcal{X} \times \mathcal{U} \rightarrow \mathcal{Z} \times \mathcal{U}$ and $\varphi^\dagger : \mathcal{Z} \times \mathcal{U} \rightarrow \mathcal{X} \times \mathcal{U}$. The corresponding manifold is $\mathcal{M} = \{\varphi^\dagger(\hat{\mathbf{z}}, \hat{\mathbf{u}}) : \hat{\mathbf{z}} \in \mathcal{Z}, \hat{\mathbf{u}} \in \mathcal{U}\} \subseteq \mathcal{X} \times \mathcal{U}$, where $\varphi^\dagger \circ \varphi(\mathcal{X} \times \mathcal{U}) = \mathcal{M}$ and $\varphi \circ \varphi^\dagger = \mathbf{id}$ (identity). For convenience, we substructure φ^\dagger by stacking the maps $\psi^\dagger : \mathcal{Z} \times \mathcal{U} \rightarrow \mathcal{X}$ and $\mathbf{id} : \mathcal{U} \rightarrow \mathcal{U}$, so that $\mathcal{M}_\mathcal{X}(\mathbf{u}_0) = \{\psi^\dagger(\hat{\mathbf{z}}, \mathbf{u}_0) : \hat{\mathbf{z}} \in \mathcal{Z}\}$. Similarly, we substructure φ into the stacked maps $\psi : \mathcal{X} \times \mathcal{U} \rightarrow \mathcal{Z}$ and $\mathbf{id} : \mathcal{U} \rightarrow \mathcal{U}$.

Based on Eq. (4), we define pointwise:

$$\mathbf{h}(\hat{\mathbf{x}}, \hat{\mathbf{z}}, \hat{\mathbf{u}}) \triangleq \hat{\mathbf{x}} - \psi^\dagger(\hat{\mathbf{z}}, \hat{\mathbf{u}}), \quad (20)$$

so that Eq. (7) writes equivalently:

$$\forall (\hat{\mathbf{x}}, \hat{\mathbf{z}}, \hat{\mathbf{u}}) \in \mathcal{M} : \mathbf{f}(\hat{\mathbf{x}}, \hat{\mathbf{u}}) - D_z \psi^\dagger(\hat{\mathbf{z}}, \hat{\mathbf{u}}) \mathbf{f}_r(\hat{\mathbf{z}}, \hat{\mathbf{u}}) = \mathbf{0}, \quad (21)$$

where we use $D_u \psi^\dagger(\cdot) \equiv \mathbf{0}$ as the derived case of $D_x \mathbf{h}(\cdot)^{-1} D_u \mathbf{h}(\cdot) \equiv \mathbf{0}$ (strict causality). As a consequence, we can redefine ψ by $\psi : \mathcal{X} \rightarrow \mathcal{Z}$ so that the encoding only depends on $\mathbf{x}(t)$. This structural restriction guarantees that $\hat{\mathbf{z}}$ is not algebraically coupled to $\hat{\mathbf{u}}$. Consequently, we will apply an AEN training that minimizes the loss $\sum_k \|\mathbf{x}^{(k)} - \psi^\dagger(\psi(\mathbf{x}^{(k)}), \mathbf{u}^{(k)})\|_2^2$. We call our approach “manifold learning with inputs” (MFLu). Next, we project \mathbf{f} onto \mathcal{M} :

$$D_z \psi^\dagger(\mathbf{z}(t), \mathbf{u}(t)) \dot{\mathbf{z}}(t) + \underbrace{D_u \psi^\dagger(\mathbf{z}(t), \mathbf{u}(t))}_{= \mathbf{0} \text{ (see above)}} \dot{\mathbf{u}}(t) = \mathbf{f}(\psi^\dagger(\mathbf{z}(t), \mathbf{u}(t)), \mathbf{u}(t)). \quad (22)$$

Finally, after left-multiplication by the pseudoinverse $D_z \psi^\dagger(\mathbf{z}(t), \mathbf{u}(t))^+$, or alternatively by $D_z \psi(\psi^\dagger(\mathbf{z}(t), \mathbf{u}(t)))$, we obtain the ROM:

$$\begin{aligned} \dot{\mathbf{z}}(t) &= D_z \psi^\dagger(\mathbf{z}(t), \mathbf{u}(t))^+ \mathbf{f}(\psi^\dagger(\mathbf{z}(t), \mathbf{u}(t)), \mathbf{u}(t)), \\ \mathbf{x}_r(t) &= \psi^\dagger(\mathbf{z}(t), \mathbf{u}(t)). \end{aligned} \quad (23)$$

This extension is related to studies on parametric model reduction; see [77, 107] for an overview. However, present works mostly deal with stationary parametric systems and use extensions of linear basis methods. In particular, [108, 109] combine a reduced POD basis and polynomial interpolation to build low-dimensional steady-state models of parametric problems. Refinements of this approach are found in [110, 111]. Reduction of parametric systems via manifold learning has also been investigated in the literature: To reduce the dimensionality of steady parametric flow problems, [112] present a strategy based on isomaps, and [113] apply kernel PCA. In [114], diffusion maps are used to learn submanifolds of the input-output space for reducing the parameter dimension. However, these works do not consider MOR of non-autonomous dynamical systems.

3.2. Non-intrusive general-purpose methods

Besides the classical intrusive reduction methods, recent advances in ML and system identification have opened new avenues toward data-driven non-intrusive model reduction [115, 116, 117]. Importantly, non-intrusive reduction does not operate on the FOM equations and is therefore “model-free”. In addition, many non-intrusive methods combine MOR and hyperreduction in a single step. However, notice that non-intrusive reduction may still exploit some structural knowledge, e.g., knowing that the FOM is a polynomial model [118]. Finally, the generic and homogeneous structure of non-intrusive ROMs can be exploited in optimization [119, 120]. As before, we disregard non-intrusive Krylov subspace methods [121, 122, 66], as these methods are not (yet) applicable to nonlinear multi-input systems.

3.2.1. Dynamic mode decomposition

Among the conceptually most simple yet effective non-intrusive methods are dynamic mode decomposition (DMD) [19] and the eigensystem realization algorithm [123], both non-intrusive linear approaches for constructing linear ROMs, i.e., linear latent dynamics on a linear subspace. Both approaches employ SVD to identify and truncate the principal linear modes from trajectory snapshot data. An extension of DMD to systems with inputs or controls (DMDc) is presented in [124], providing a ROM:

$$\begin{aligned} \mathbf{z}(k+1) &= \mathbf{A}\mathbf{z}(k) + \mathbf{B}\mathbf{u}(k), \\ \mathbf{x}_r(k) &= \mathbf{U}_1\mathbf{z}(k), \end{aligned} \quad (24)$$

where $\mathbf{U}_1 \in \mathbb{R}^{n_x \times n_z}$, $\mathbf{A} \in \mathbb{R}^{n_z \times n_z}$, and $\mathbf{B} \in \mathbb{R}^{n_z \times n_u}$. We refer to [124] for details on the computation of \mathbf{A} , \mathbf{B} , and \mathbf{U}_1 . For a stable linear FOM, [125] presents bounds on the prediction error, $e(k) \triangleq \mathbf{x}_r(k) - \mathbf{x}(k)$, for $k > N$. However, as discussed in [126], DMDc may struggle with significantly nonlinear systems.

3.2.2. Applied Koopman theory

An extension of the DMD algorithm (EDMD) was proposed in [33]. Their approach still provides a linear ROM, but the mathematical procedure to construct the dynamics involves a prior nonlinear lifting step based on Koopman theory. Koopman theory [32, 127] postulates that a nonlinear dynamical system possesses a linear operator representation when lifted to a generally infinite-dimensional space of observables $g : \mathcal{X} \rightarrow \mathbb{C}$. Constructing a finite-dimensional or even low-order Koopman model by means of (E)DMD corresponds to a Galerkin projection of the Koopman operator onto a set of basis functions g_i , collected in \mathbf{g} . Hence, despite being a linear method, DMD is applicable to nonlinear systems, when substituting state snapshots $\mathbf{x}^{(k)}$ by a sufficiently rich set of embedded snapshots $\mathbf{g}(\mathbf{x}^{(k)})$. Common choices of real-valued observables include Hermite polynomials, radial basis functions, sparse regression, and ANNs [33, 128]. More recently, kernel methods have gained attention due to their strong approximation capabilities [129, 130, 131].

Notably, a Koopman model does not necessarily predict states but only deals with observables. However, we can adapt the Koopman framework to state prediction by demanding that $\mathbf{x}(t)$ can be inferred from $\mathbf{g}(\mathbf{x}(t))$. To this end, a common assumption is that $\mathbf{x}(t)$ can be linearly reconstructed from the nonlinear observables. For example, [132] and follow-ups [133, 134, 135] use EDMD with inputs or controls (EDMDc):

$$\begin{aligned}\dot{\mathbf{z}}(t) &= \mathbf{A}\mathbf{z}(t) + \mathbf{B}\mathbf{u}(t), \\ \mathbf{z}(t_0) &= \mathbf{g}(\mathbf{x}(t_0)), \\ \mathbf{x}(t) &= \mathbf{C}\mathbf{z}(t),\end{aligned}\tag{25}$$

where $\mathbf{z}(t) \in \mathbb{R}^{n_z}$ are the Koopman states, $\mathbf{g} : \mathcal{X} \rightarrow \mathbb{R}^{n_z}$ is the nonlinear observable map, and $\mathbf{A} \in \mathbb{R}^{n_z \times n_z}$, $\mathbf{B} \in \mathbb{R}^{n_z \times n_u}$, $\mathbf{C} \in \mathbb{R}^{n_x \times n_z}$. A ROM is obtained when setting $n_z < n_x$.

In the past years, Koopman theory has become a popular approach for both model bilinearization [136, 137, 138] and non-intrusive MOR [139, 140]. For autonomous systems, [141] relaxes the assumption of a global linear projection and proposed to combine linear dynamics and nonlinear reconstruction by means of a decoder network \mathbf{g}^\dagger . In [51], we have shown that this strategy is also valid for input-affine systems. Under certain assumptions on the observables \mathbf{g} (see [51]), the respective ROM takes the form:

$$\begin{aligned}\dot{\mathbf{z}}(t) &= \mathbf{A}\mathbf{z}(t) + \mathbf{B}\mathbf{u}(t), \\ \mathbf{z}(t_0) &= \mathbf{g}(\mathbf{x}(t_0)), \\ \mathbf{x}_r(t) &= \mathbf{g}^\dagger(\mathbf{z}(t)),\end{aligned}\tag{26}$$

which is visualized by Fig. 3. Notice that the linear dynamics in Eq. (26) is a special case of the bilinear dynamics derived in [51]. For non-oscillating systems, we may choose a diagonal \mathbf{A} and thereby reduce the trainable parameters. The combination of linear dynamics and nonlinear static map has ‘‘Wiener structure’’ and we term Eq. (26) a ‘‘Koopman-Wiener’’ (KW) model. In contrast to Eq. (19), we do not only project the nonlinear dynamics onto some subspace of \mathcal{X} , but we additionally demand the projection \mathbf{g} to be linearizing. Consequently, the learning problem is more complex than standard MFL. Realizing the KW framework is most straightforward in a non-intrusive fashion, where an ML training combines reconstruction, prediction, and regularization loss terms [51]. Finally, the flexibility of ML enables modifications of the KW structure. For example, the encoder may serve as a state estimator [142].

3.2.3. Lift-and-project methods

Lift-and-project methods expand the FOM into an even higher-dimensional canonical form before projecting this representation to a low-dimensional subspace. The lifting step usually targets a linear,

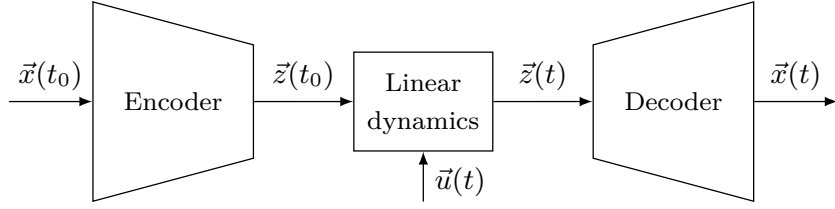


Fig. 3: Model structure of the Koopman-Wiener ROM.

bilinear, or quadratic representation of the FOM. This extra step enables (i) the use of linear or bilinear MOR methods, and (ii) circumvents hyperreduction due to mathematically simpler ROMs. Methods such as Koopman lifting [143], Carleman bilinearization [144], piecewise linearization [145] or Taylor expansion [29, 30, 31], lay the theoretical foundation of lift-and-project methods.

Because intrusive variants of lift-and-project methods are mathematically involved and computationally expensive, non-intrusive implementations are convenient to circumvent lifting the FOM. For example, the studies [118, 146] presented a non-intrusive lifting method for polynomial FOMs, where snapshot data is lifted and POD-projected to learn a quadratic ROM. Therein, the model regression of the quadratic ROM is called “operator inference” (OPI) [147, 148]. However, this lift-and-learn method [118, 146] currently requires the manual (pen-and-paper) derivation of the candidate lifting maps.

3.2.4. Reduced basis and manifold learning methods

An alternative non-intrusive reduction approach is to combine reduced basis methods or manifold learning with system identification methods. For example, given POD-reduced snapshots, the latent ROM dynamics may be learned using recurrent neural networks (RNNs) [149], temporal convolutional ANNs [150], or feedforward ANN predictors [151]. Analogously, given AEN-compressed snapshots, an ROM can be obtained, e.g., using RNNs [152] or Hammerstein-Wiener models [153]. These approaches are non-intrusive counterparts to Eq. (19).

The above methods are two-stage procedures because the slow manifold is constructed independently of the latent dynamics. However, this separation may introduce a bottleneck, i.e., the latent variables may not be suitable latent states, depending on the type of predictor. Interestingly, a similar bottleneck is also present in intrusive model reduction, as highlighted in [154, 104]. Non-intrusive single-stage approaches address this issue by learning slow manifold and latent dynamics simultaneously. Conveniently, the KW method reviewed above inherently follows this strategy [51]. In a similar but empirical setup, the works [155, 156] use AENs and linear time-invariant dynamics to learn stochastic ROMs. Alternative approaches combine MFL and RNNs [157], MFL and feedforward ANNs (termed MFL-ANN below) [158, 159, 160], or MFL and sparse identification of latent dynamics [161].

3.3. Discussion and comparison

We present a theoretical comparison of the reviewed methods with respect to their nonlinear reduction properties in Table 1. First, we distinguish methods by their intrusive character (**Intr**). Intrusive MOR methods do not inherently perform hyperreduction (**Hr**) and thus require additional model simplification efforts for real-time applications. In contrast, non-intrusive methods use ROM structures that are typically (by design) much cheaper to evaluate so that a separate hyperreduction step is not needed.

Next, we distinguish whether the methods are snapshot-based (**Snap**). This categorization reveals another practical limitation (**NU**). Snapshot-based methods usually face the curse of dimensionality

Table 1: Comparison of nonlinear MOR methods that preserve state information. **Intr**: intrusive method, **Snap**: snapshot-based method, **Manif**: type of submanifold, **Lat**: type of latent dynamics, **Hr**: hyperreduction features, **Nu**: suitable for many inputs ($n_u \gg 1$), **Ctr**: approximates controllable subspace, **Stab**: preserves stability. (✓) practical limitations.

Method	Section	Intr	Snap	Manif	Lat	Hr	Nu	Ctr	Stab
a) POD-Galerkin	3.1.1	✓	✓	Lin.	Nonlin.	✗	(✓)	✓	✗
b) SPT	3.1.2	✓	✗	Nonlin.	Nonlin.	✗	✓	✗	✓
c) POD-Res.	3.1.3	✓	✓	Nonlin.	Nonlin.	✗	(✓)	✓	✓
d) MFL-Galerkin	3.1.4	✓	✓	Nonlin.	Nonlin.	✗	(✓)	✓	✗
e) MFLu-Galerkin	3.1.5	✓	✓	Nonlin.	Nonlin.	✗	(✓)	✓	✗
f) DMDc/EDMDc	3.2.1/2	✗	✓	Lin.	Lin./Bilin.	✓	(✓)	✓	✗
g) KW	3.2.2	✗	✓	Nonlin.	Lin./Bilin.	✓	(✓)	✓	✓
h) OPI	3.2.3	✗	✓	Lin.	Quadr.	✓	(✓)	✓	✓
i) POD-ANN/RNN	3.2.4	✗	✓	Lin.	Nonlin.	✓	(✓)	✓	✗
j) MFL-ANN/RNN	3.2.4	✗	✓	Nonlin.	Nonlin.	✓	(✓)	✓	✗

in n_u , since an independent excitation of inputs is commonly used to adequately cover the relevant state-space regions. As a consequence, snapshot-based methods are less straightforward to apply to systems with many inputs, i.e., $n_u \gg 1$. Hence, for systems with many independent inputs $\mathbf{u}(t)$, snapshot-free intrusive methods are the most suitable.

Despite the curse of dimensionality, input-response snapshots contain valuable information about controllability. As discussed in [162], when the snapshots are created via broad excitation of the system through the inputs, these data sample the controllable subspace. As a consequence, building a ROM based on input-response data inherently approximates the controllable subspace and eliminates the uncontrollable states (**Ctr**).

Next, we distinguish between methods that construct a linear (or affine) subspace versus a nonlinear manifold (**Manif**). As discussed in Section 1, using a linear subspace can limit the possible degree of reduction. On the other hand, computing a reduced basis by means of POD is numerically robust and computationally cheaper than MFL. The effort of a system-theoretic reduction, such as SPT, depends on the system knowledge and availability of heuristics. Overall, there is a trade-off between reduced order and reduction effort.

Lastly, we distinguish the reduction methods by the type of latent dynamics (**Lat**), see Eq. (4a). In general, the ROM of a nonlinear FOM is also nonlinear. However, DMDc and KW reduction methods construct linear latent dynamics, whereby the nonlinear ROM is simplified and “structurally regularized”. In other words, a ROM with linear latent dynamics cannot falsely exhibit strong nonlinear phenomena such as chaos or state multiplicity [163]. At the same time, these ROMs are limited to mildly nonlinear systems or short prediction horizons. However, a ROM with linear or bilinear latent dynamics is oftentimes sufficient, where more complex structures, e.g., MFL-ANN, bear a higher risk of overfitting and undesired dynamical behavior.

Relatively few nonlinear model reduction methods provide a-priori guarantees on stability preservation (**Stab**). These guarantees are established by system-theoretic arguments (SPT, AGG, POD-Res.) or through constrained learning problems (KW, OPI). Other methods require a careful a-posteriori investigation of stability properties of the ROM [77]. Regarding the ROM error, $\mathbf{e}(t) \triangleq \mathbf{x}_r(t) - \mathbf{x}(t)$, available nonlinear MOR techniques usually do not provide universal error bounds but require a-posteriori ROM validation. Special MOR methods that provide error bounds for special types of nonlinear systems have been presented, e.g, in [164, 165].

4. Reduced modeling of chemical processes

We now review specialized MOR methods developed in the PSE field as well as applications of general-purpose methods to PSE problems. In Section 4.1, we review three specializations of MOR methods from the previous section, namely (i) compartment modeling, (ii) model aggregation, and (iii) collocation method. Afterwards, in Section 4.2, we discuss the application of MOR to three very common unit operations: (i) distillation columns, (ii) heat exchangers (HX), and (iii) reactors. Again, we omit equations as far as possible and rather focus on an abstract discussion. Besides deterministic reduction, reduced modeling is often achieved based on knowledge or intuition through simplifying assumptions in the modeling process [166]. We also comment on these aspects.

4.1. Problem-specific approaches

4.1.1. Compartment modeling

The key concept in compartment modeling (COMP) is the definition of interconnected functional subsystems, termed “compartments”, between the local microscale and the global system scale [167]. When applied for MOR, the introduction of compartments is often motivated by a time scale assumption, where local phenomena inside a compartment are assumed to be much faster than the overall response of the compartment [85]. Given a discretized model of a conservative distributed system, a compartment is a cluster of neighboring cells, and the compartment equations are obtained by superposition of the extensive balance equations, e.g., absolute enthalpy or total molar holdup, of these cells. In terms of intensive quantities, e.g., molar enthalpy and molar fraction, this superposition corresponds to a mass-weighted averaging.

By applying the above time scale assumption, the local dynamics of cells within a compartment are degenerated to quasi-stationary equations, and we obtain a ROM. In addition, replacing quasi-stationary equations by shortcut methods, averaging rules, or regression models realizes a hyperreduction. COMP is a heuristic approach to transform an FOM into Eqs. (12) and (13). Hence, we regard COMP as a heuristic SPT method, inheriting properties such as the potential appearance of a non-physical IR (see discussion below).

4.1.2. Model aggregation

In order to eliminate the potential IR in COMP ROMs and improve model sparsity, [168] presents the “aggregation method” (AGG). AGG is a heuristic modification of SPT for 1D distributed systems. Instead of transforming the FOM into the canonical form (12), the authors multiply (only) the left-hand side of the FOM by a matrix $\tilde{\mathbf{H}} = \text{diag}(\tilde{h}_1, \tilde{h}_2, \dots, \tilde{h}_{n_x})$, $\tilde{h}_i \geq 0$. Thereby, the time constants of individual stage dynamics are artificially increased or reduced. $\tilde{\mathbf{H}}$ is a hyperparameter and commonly $\text{trace}(\tilde{\mathbf{H}}) \approx n_x$. Let Ω be the $n_x \times n_x$ permutation matrix such that $\Omega \tilde{\mathbf{H}} = \begin{bmatrix} \mathbf{H} & \mathbf{0} \\ \mathbf{0} & \mathbf{0} \end{bmatrix}$, where $\mathbf{H} = \text{diag}(h_1, h_2, \dots, h_{n_x})$, $h_i > 1$. The resulting ROM reads:

$$\mathbf{H} \dot{\mathbf{x}}_1(t) = \mathbf{f}_1(\mathbf{x}_1(t), \mathbf{x}_2(t), \mathbf{u}(t)), \quad (27a)$$

$$\mathbf{0} = \mathbf{f}_2(\mathbf{x}_1(t), \mathbf{x}_2(t), \mathbf{u}(t)). \quad (27b)$$

A systematic comparison of AGG to COMP is given in [169]. By contrasting Eqs. (13) and (27), we notice that the manifolds on which the ROMs evolve are identical if \mathbf{f}_2 coincide. Hence, both methods may realize a different ROM living on the same manifold \mathcal{M} .

4.1.3. Collocation method

Motivated by the collocation method for solving ODEs and PDEs [170, 171], the studies [8, 172] adapt the collocation method to MOR of spatially discrete (staged) problems. The underlying assumption is a polynomial coherence of the differential variables of the FOM. Then, a ROM is obtained by combining polynomial interpolation and a number of discrete cells (collocation points), e.g., finite

volume elements or column stages. However, the collocation points do not necessarily correspond to cells in the FOM. Intuitively, the number and position of collocation points depend on the system, i.e., whether a low-order polynomial is able to capture the underlying pattern (slow manifold). The positions of the collocation points are typically chosen a-priori as the roots of Legendre, Hahn, or Jacobi polynomials and not further adapted online [173, 174]. In other words, the spatial collocation points are determined once and for all, i.e., do not change over time.

4.2. Applications

4.2.1. Distillation columns

Detailed distillation column models typically include “stage-by-stage” differential energy, mass, and possibly momentum balances [175]. Common simplifying assumptions are ideally mixed stages with no diffusion effects, thermodynamic vapor-liquid equilibrium, and quasi-stationary pressure and enthalpy dynamics of both phases [86, 82]. These assumptions rely on time-scale assumptions and may be regarded as a heuristic application of SPT, rendering such mechanistic models already reduced. However, these models are often too expensive for online applications and therefore require MOR [176, 177].

Early applications of MOR to columns are found in [8, 172] for COL and [178] for COMP. As mentioned above, when applying COL, the collocation points do not necessarily correspond to physical separation stages, i.e., can be pseudo-stages. Moreover, constructing COL models based on a log-transformed FOM can improve model accuracy [179].

Using SPT, [85] derives a widely applicable COMP model form and shows a higher accuracy over COL. The COMP ROMs therein combine dynamic compartment balances and quasi-stationary stage models. The separation stage whose differential balances are replaced by compartment balances is termed “sensitivity stage”. The appearance of a non-physical IR depends on the number of compartments and the position of the sensitivity stages [87, 180]. However, avoiding an IR may limit the degree of order reduction. On the other hand, the particular structure of COMP models, featuring large sets of neighboring quasi-stationary stage models, enables hyperreduction via steady-state shortcut methods, e.g., FUG shortcut [46] or group methods [181, 182]. Typically, these shortcuts have fewer parameters than universal regressors (e.g., ANNs) and are less prone to overfitting. On the other hand, ANNs can reach almost arbitrary precision [183].

In steady operation, a distillation column exhibits a set of coherent composition patterns, which can be analytically derived under simplifying assumptions [184, 185]. These analytical solutions are wave-shaped profiles, and therefore called “nonlinear wave propagation model” (NWPM). [186] proposed a semi-empirical ROM for multi-species distillation columns, by combining NWPM equations, global column balances, and a boundary equilibrium assumption. The resulting NWPM-ROM is a compartment model (a non-physical IR is also observed here). In [187], this ROM was extended to account for effects due to non-constant holdup.

The AGG method was originally developed for distillation columns [168]. Like COMP models, AGG ROMs involve clusters of quasi-stationary trays that can be simplified using shortcut models. Different from COMP, the AGG ROM states may be associated with actual stages in a distillation column. While avoiding a non-physical IR, the AGG states usually converge more slowly to the FOM states after a change of system inputs [188].

Besides the specialized MOR methods, general-purpose MOR methods have been applied to distillation column models, e.g., using POD-Galerkin [61, 189], standard SPT [190], KW [142, 120], and DMDc [191]. However, as opposed to these general-purpose methods, the specialized methods, COMP (including NWPM), AGG, and COL, build on the intrinsic system structure, providing generic low-order models that can be written (almost) independently of a FOM. In particular, these specialized methods can be pre-configured for generic columns with similar stage models and in many cases steady-state data is sufficient to configure these ROMs for a specific column. Moreover, COMP and AGG may access an extra set of hyperreduction methods in the form of steady-state shortcuts as described above.

4.2.2. Heat exchangers

HX are another type of distributed systems that are commonly associated with high-order FOMs. For industrial processes, the 3D discretized model of a multi-stream HX can reach an order of over a million states [9]. Clearly, such fine-grained models are prohibitive for real-time applications.

As an alternative to MOR, simplifying assumptions enable a heuristic degeneration or lumping of differential equations. Common assumptions are (i) a time scale separation between energy dynamics of fluids and walls and (ii) for parallel flow HX, a uniform “common wall” temperature in each cross section perpendicular to the principal flow axis [192]. Common examples of lumped parameter models are ε -NTU, P-NTU and LMTD [193]. However, these are typically only valid at stationary points and under simplified assumptions on geometry, heat transfer, and thermodynamics.

Under reasonable simplifying assumptions, such as constant heat capacities and linear heat transfer correlations, the HX FOMs are (quasi-)linear or bilinear [194]. In that case, linear or bilinear MOR may be applied [195], which is less involved than general nonlinear MOR. Moreover, when including dynamical HX submodels in a process model, the heat transfer phenomena often have significantly smaller time constants than mass conversion and mass transfer problems [196]. Under these assumptions, a dynamical HX model may fully degenerate into a quasi-stationary model.

Applications of general-purpose MOR methods to HX include POD-Galerkin [197, 198, 199], DMD [200], and POD combined with ANNs/RNNs [201]. Furthermore, both classical collocation and Galerkin projection are standard methods to approximate low-order solutions of HX PDE models [202, 193]. In addition, all three specialized approaches (COMP, AGG, COL) have been applied to spatially discretized dynamical models of 1D distributed HX. Specifically, [179, 203] use the collocation method to reduce finite volume models of HXs. Lumped COMP models of HX are presented in [204, 205, 206]. Also, the reduced modeling of HX with phase change (evaporators or condensers) is often accomplished using the “moving boundary model” (MBM) [207], which is a COMP model. The MBM uses compartments with flexible boundaries to account for spatially moving phase regions and can exhibit a non-physical IR [208]. Finally, AGG is applied to HX in [209].

Similar to separation columns, there exist steady-state shortcut models and analytic solutions to replace steady-state equations in COMP and AGG models. Common lumped parameter models are reviewed in [193]. Refs. [194] presents an analytic solution to the stationary multi-stream HX equations under simplifying assumptions. Further, HX networks may be used as a surrogate model of multi-stream HX [210, 211].

4.2.3. Reactors

There are two main aspects that can result in high-order FOMs of chemical reactors. First, reaction systems can include high-dimensional multispecies kinetics with numerous reaction pathways [212, 213, 214]. Second, the spatial distribution of a reactor can prohibit lumped models, e.g., for non-ideally mixed tanks or for tubular reactors [17, 215].

For kinetic systems, a reduction in the number of species corresponds to MOR, whereas a reduction in the number of modeled reactions may be regarded as hyperreduction. Analogously to the simplifying assumptions discussed for column and HX modeling, the FOM of a kinetic system is often already a simplification of the real mechanisms and so is the mechanistic model of a reactor. Naturally, for two-timescale kinetic systems with a clear partitioning between slow and fast dynamics, SPT can be directly applied [216].

A large set of works has been devoted to constructing the invariant manifolds by approximately solving the invariance equations of chemical kinetic systems with non-obvious slow and fast partitioning. These

methods employ system linearization [212], computational singular perturbation [217], thermodynamic dissipativity and symmetry [218] relation graphs [219, 220], or sensitivity analysis and numerical optimization [221, 222, 223]. Extensive reviews are given in [224, 225, 226]. Recently, ML methods have been increasingly applied to reduce kinetic systems [227, 228, 229, 230].

For spatially distributed reaction systems, e.g., reaction diffusion problems and tube reactors, the application of POD-Galerkin method [231, 232, 215, 233], nonlinear-Galerkin method [234, 13, 17], manifold-Galerkin method [36], and lift-and-reduce techniques [118] have been reported. As shown in [36], nonlinear subspace methods can significantly outperform linear basis methods in the very-low-order region. The classical collocation method is applied, e.g., in [235, 10, 236], to obtain low-order solutions of respective PDEs models. Moreover, an overview of compartment modeling of distributed chemical reactors is found in [237].

For integrated reaction-separation systems (with recycle), the works [238, 239] performed a time scale analysis by means of SPT to derive ROMs for control. Along the same lines, [196] investigated integrated reaction-heat exchange networks. Ref. [60] compared the POD-Galerkin and POD-Res method on an integrated reaction-separation system, finding similar ROM accuracy but higher CPU costs of POD-Res ROMs.

5. Case study

We compare the performance of MOR methods on an industrial process by studying the ASU presented in [240]. Clearly, comparing all the methods reviewed in Sections 3 and 4 would exceed the scope of this article. Hence, we examine a subset of methods listed in Table 1. Specifically, we compare the MOR approaches (a-g) and (j). Additionally, we consider the two tailored methods COMP and AGG from Section 4.

We briefly comment on the method selection. Despite successful applications in the literature, we neither investigate COL nor NWPM, because low-order COL models are known to exhibit a significant steady-state offset [85] and NWPM is a special case of COMP. We refer to [179] and [187] for applications of COL and NWPM to the ASU considered herein, respectively. Furthermore, we do not investigate OPI (h) due to the intricate “pen-and-paper” lifting [146]. Of the many possible approaches (i) and (j) reviewed in Section 3.2.4, we choose the MFL-ANN method [159] due to conceptual simplicity and low implementation efforts. Further, class (i) is theoretically included in (j) and therefore not investigated separately. In particular, we expect all single-stage methods in Section 3.2.4 to reach a comparable accuracy. Finally, recall that POD-Res and COMP represent data-driven and heuristic variants of SPT, respectively. In this regard, our case study covers SPT. As discussed in Section 1, we focus on MOR and do not investigate a potential hyperreduction and CPU times.

Fig. 4 illustrates the ASU under investigation, which produces gaseous nitrogen and is built of a main air compressor (MAC) with precooling, three multi-stream HXs, two turbines (T1, T2), a high-pressure rectifying column (HPC) with 30 trays, and an integrated reboiler condenser unit (IRC). The ASU has four manipulated variables (MVs), which are the molar flow rate of air F_{mac} , the molar flow fraction to the turbine ζ_{turb} , the reflux fraction at the column top ζ_{cond} , and the purge stream F_{drain} .

The ASU is open-loop unstable due to the integrator behavior of the liquid molar holdup M_{irc} of the IRC. For unstable processes, data sampling is more challenging, especially if only a small subregion of the state space is relevant for ROM application. However, most chemical plants feature a stabilizing base layer as part of the automation hierarchy, so stability is not an issue [241]. For simplicity, we thus assume that the IRC is equipped with an ideal inventory controller that manipulates F_{drain} to stabilize M_{irc} at its nominal value. Additionally, we fix ζ_{turb} to its nominal value. Consequently, we have two variable inputs $\mathbf{u} = [F_{\text{mac}}, \zeta_{\text{cond}}]^T$.

For our purpose, the selected ASU features some characteristic properties of industrial process systems, such as variable coupling and nonlinear process response. Moreover, we regard the ASU as a good

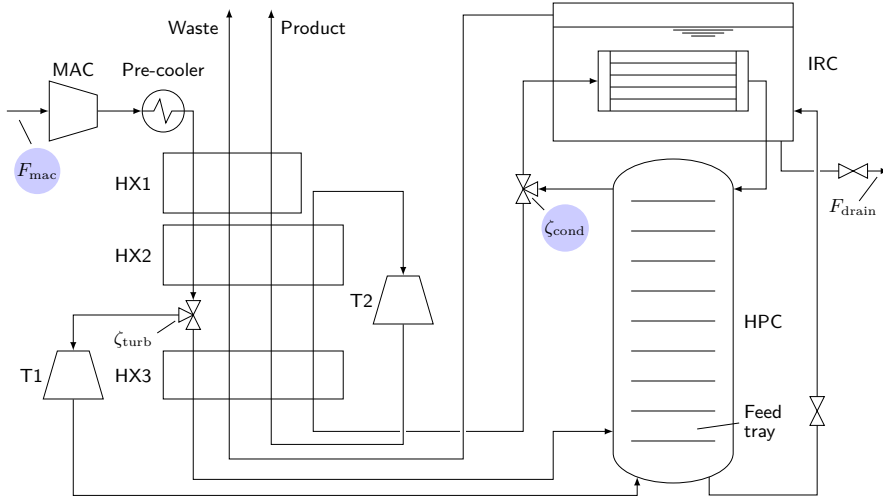


Fig. 4: Process flowsheet of the ASU: Heat exchangers (HX), high-pressure column (HPC), reboiler tank (IRC), compressor (MAC), and turbines (T). Blue circles indicate inputs $u(t)$.

compromise between the complexity of the process system and the complexity of the MOR problem. However, the selected process does not incorporate a chemical reactor and has few inputs. The investigation of MOR for complex processes including reaction and many MVs is indispensable and should be undertaken in future studies.

5.1. Full-order model

We consider the three main species of air nitrogen, argon, and oxygen. In contrast, we do not model carbon dioxide, hydrocarbons, or other residual chemical species here. The FOM of the ASU comprises material and energy balances of all process units as well as constitutive equilibrium-based thermodynamic equations. The HPC is modeled in a tray-to-tray fashion assuming thermal equilibrium with constant relative volatilities, constant specific heat capacities of all species, and ideal mixture (no excess properties). Both the HPC bottom tray and the IRC reboiler are modeled as special column trays with an extra feed stream and fixed liquid outflow, respectively. The IRC condenser is a total condenser with negligible material holdup and modeled using lumped quasi-stationary balance equations. We apply a logarithmic transformation of molar fractions to support the extraction of composition patterns, i.e., the logarithmic molar fractions are the respective differential states. The HX models feature energy balances for the metal wall and quasi-stationary balances for the fluids, assuming a single stream layer each, 1D spatial discretization with n_{HX} cells per stream, and the common wall assumption. Following [240], we set $n_{HX1} = 25$, $n_{HX2} = 25$, and $n_{HX3} = 1$. Lastly, first-order low-pass filters account for the lagged vapor flow rate in HX and HPC.

In total, the FOM comprises $n_u = 2$ inputs and $n_x = 176$ differential states, and is implemented in **Modelica**. The admissible input set \mathcal{U} is a box defined by $F_{mac} \in [30 \text{ mol/s}, 50 \text{ mol/s}]$ and $\zeta_{cond} \in [0.51, 0.54]$. As the initial state \mathbf{x}_0 , we use the nominal steady state corresponding to $F_{mac} = 52.2 \text{ mol/s}$, $\zeta_{cond} = 0.535$, $\zeta_{turb} = 0.805$, and $M_{irc} = 25 \text{ kmol}$. At \mathbf{x}_0 , the ASU produces 25 mol/s nitrogen of 100 ppm impurity grade.

5.2. Data sampling

In order to guarantee a fair comparison of snapshot-based methods against each other, we always use the same training data. This data set is recorded by simulating the FOM subject to randomly ordered inputs drawn from an equidistant 5×5 grid in \mathcal{U} . Following [240], the sampling time is $\Delta t_s = 15 \text{ min}$. We impose the input sequence as steps (zero-order hold) of 240 h (10 days) duration. Thereby, we include information from both the fast spectrum of the system response and the stationary states. We illustrate the input profile $\mathbf{u}(t)$ in the supplementary information (SI).

We simulate the FOM in **Dymola** 2025x using the integrator **DASSL** [242] with integration tolerance 10^{-6} . The recorded data set comprises $N = 24\,000$ snapshots of each state. The corresponding snapshot matrices have the form $\mathbf{X} \in \mathbb{R}^{n_x \times N}$ and $\mathbf{U} \in \mathbb{R}^{n_u \times N}$. These snapshots cover the operating space between 15 mol/s and 27 mol/s production rate and product quality between 10 ppm and 1000 ppm impurities.

5.3. Implementation

As previously discussed, POD and MFL are strongly affected by scaling. Herein, we scale all states and inputs individually to the range $[-1, 1]$ and apply zero-mean centering. We remark that a tailored scaling strategy, e.g., scaling based on physical relevance and range, may enable more accurate ROMs (with respect to a target application). Like the FOM, we implement all intrusive ROMs in **Modelica** and perform all simulations in **Dymola** using **DASSL** with an integration tolerance of 10^{-6} . The non-intrusive ROMs (DMDc, KW, MFL-ANN) are directly evaluated in the respective ML environments in **Python** (see below). Next, we provide further details on the implementation.

5.3.1. POD methods and DMDc

We implement POD and DMDc using **SciPy** as a **Python** interface to the SVD implementation in **LAPACK**. All other matrix computations are performed using **Numpy**. We specify **float64** precision, which was found to be crucial for obtaining reliable SVD results. We scale the latent states $\mathbf{z}(t)$ heuristically, which was found to improve model conditioning. For DMDc, we calculate the coefficient matrices \mathbf{A} , \mathbf{B} , and \mathbf{U}_1 in Eq. (24) using the formulas given in [124]. To derive a POD-Res model, we use a truncated residualization, where $n_q = 50 - n_z$. The truncation improves simulation convergence without significant loss of precision.

5.3.2. MFL-Galerkin and MFLu-Galerkin methods

We train AENs in **Tensorflow** using the standard training problem with MSE reconstruction loss [102]. To reduce the number of trainable parameters and speed up the training, we prereduce the scaled and zero-centered snapshots by projecting the data onto the first 100 POD modes [101]. For the success of MFL, it is crucial to not rescale the projected snapshots again. The encoders and decoders have a single fully connected nonlinear hidden layer with 50 neurons with (smooth) **tanh** activation, respectively. Using deeper networks or additional neurons did not improve the reconstruction accuracy considerably.

We divide the pre-processed snapshots into 80 % training data and 20 % validation data. For every network, we run three trainings with random seeds and select the weights with the best performance on the validation data set. We train all networks for a total of 20 000 epochs and minibatch size 256, using **Adam** with initial learning rate (LR) of 10^{-4} for the first 15 000 epochs and **SGD** with LR of 10^{-6} for subsequent finetuning. For the implementation of MFLu, we modify the AEN structure from $(\varphi, \varphi^\dagger)$ to (ψ, ψ^\dagger) as discussed in Section 3.1.5. However, the general training setup remains the same. To include the AENs in the ROMs, we implement the decoder network structure in **Modelica**.

5.3.3. KW models

We use our ML framework [51] to train reduced KW models. This framework is based on **Tensorflow** and implements the KW model structure along with a training procedure based on snapshot data. As in Section 5.3.2, we pre-reduce the training data through projection onto the principal 100 POD modes. The trajectory snippets required for the prediction loss are created by sliding along the training data set in a moving horizon fashion, stopping every 10 samples and copying a series of 100 consecutive snapshots. The encoder and decoder networks have a symmetric structure with two hidden layers and linear output layer. The number of hidden neurons are determined via linear interpolation between 100 and n_z . We use **ELU** activation and train the model for 10 000 epochs and minibatch size 32, where the first 8 000 epochs use **ADAM** with LR of 10^{-3} and the final 2 000 epochs use **SGD** with LR of 10^{-6} for finetuning. All other hyperparameters have the default values from [51]. The ROM simulation employs the graph-based execution mode of **Tensorflow**.

5.3.4. MFL-ANN models

We implement the method in [159] by means of a modification of our aforementioned framework [51]. To this end, we substitute the linear dynamics in Eq. (26) by a feedforward ANN to learn the discrete-time latent predictor:

$$\mathbf{z}_{k+1} = \mathbf{F}(\mathbf{z}_k, \mathbf{u}_k), \quad (28)$$

where $\mathbf{F} : \mathcal{Z} \times \mathcal{U} \rightarrow \mathcal{Z}$ and $k \in \{0, 1, \dots\}$. The ANN \mathbf{F} features two hidden layers of each $2n_z$ neurons and ReLU activation, and a linear output layer. This specification is parsimonious compared to [159], who use three hidden layers of each $5n_z$ neurons. However, we found that overparameterization results in poor training convergence. All other settings, including AEN structure and training hyperparameters, are identical to Section 5.3.3.

5.3.5. COMP and AGG models

Both methods are applied to the ASU process model in a unit-by-unit fashion. However, the submodels of HX3, HPC feed stage, and IRC already have a minimal form and cannot be further reduced by the COMP or AGG. Since the dynamic relevance of these units is unclear without further investigation, we leave them untouched. Moreover, preliminary experimentation showed that the HX dynamics have a noticeable effect on the overall system response. Hence, we do not replace these units by quasi-stationary models, i.e., we create and insert ROM submodels for HX1, HX2, and HPC.

The number and size of compartments and the position of the sensitive elements (referring to HPC trays and HX cells simultaneously) are degrees of freedom of the COMP method and may be regarded as hyperparameters. Similarly, the hyperparameters of AGG are the number and positions of aggregation elements. We follow [183] and use compartments of a uniform size, with sensitive elements located in the center of the respective compartments. A perturbation analysis of the positions confirmed this choice. We select the same central positions for the aggregation elements. Using the same number of compartments or aggregation elements n_c for each HX1, HX2, and HPC, we obtain $n_z = 10 + 6 \cdot n_c$. In all AGG models, we specify \mathbf{H} in Eq. (27) such that $\text{diag}(\mathbf{H}) = n_x$.

5.4. Definition of the comparison criteria

We compare the selected MOR techniques in two tests. First, we only assess the accuracy of the linear or nonlinear subspaces, i.e., the slow manifold approximations, constructed by the MOR methods. This assessment does not yet include ROMs, but merely determines the average accuracy of projecting the FOM state snapshots of a test data set onto the respective low-dimensional subspaces. In particular, the projection error constitutes a lower bound on the ROM prediction error [22]. Second, we simulate the ROMs, i.e., we examine the prediction capabilities of the ROMs. This prediction test is the most important criterion as we assess the overall ROM accuracy. We initialize all ROMs at the nominal steady state described above.

In both evaluations, we use an independent test data set that comprises a series of random uniformly distributed zero-order hold inputs (illustration see SI). Furthermore, we consider different degrees of reduction, i.e., we vary the reduced order n_z . As previously discussed, for COMP and AGG, the values of n_z are not freely selectable but are restricted by the subsystem-by-subsystem application of the methods, where viable options are $n_z \in \{16, 22, 28, \dots\}$. To facilitate a comparison of the MOR methods, we include such values of n_z into the study.

We evaluate the accuracy in terms of the root mean squared error (RMSE), which we define in terms of the Frobenius norm:

$$\text{RMSE}(\mathbf{X}, \mathbf{X}_r) \triangleq \sqrt{\frac{1}{n_x N} \|\mathbf{X} - \mathbf{X}_r\|_F^2}. \quad (29)$$

Table 2: Results of projection accuracy. The RMSE indicates the average error between the states projected on the reduced subspace versus the original FOM states. We consider different ROM orders n_z .

n_z	POD/DMDc	POD-Res	MFL	MFLu	KW	MFL-ANN	COMP	AGG
2	$7.8 \cdot 10^{-2}$	$4.9 \cdot 10^{-2}$	$1.0 \cdot 10^{-2}$	$5.3 \cdot 10^{-3}$	$1.5 \cdot 10^{-1}$	$1.6 \cdot 10^{-1}$	—	—
5	$1.6 \cdot 10^{-2}$	$1.7 \cdot 10^{-2}$	$2.2 \cdot 10^{-3}$	$1.8 \cdot 10^{-3}$	$1.4 \cdot 10^{-2}$	$2.5 \cdot 10^{-2}$	—	—
10	$3.8 \cdot 10^{-3}$	$1.2 \cdot 10^{-2}$	$1.3 \cdot 10^{-3}$	$1.4 \cdot 10^{-3}$	$7.3 \cdot 10^{-3}$	$2.5 \cdot 10^{-2}$	—	—
16	$1.1 \cdot 10^{-3}$	$5.5 \cdot 10^{-3}$	$7.3 \cdot 10^{-4}$	$1.5 \cdot 10^{-3}$	$6.1 \cdot 10^{-3}$	$1.5 \cdot 10^{-2}$	$9.4 \cdot 10^{-2}$	$4.8 \cdot 10^{-2}$
28	$9.0 \cdot 10^{-5}$	$3.6 \cdot 10^{-3}$	$1.4 \cdot 10^{-3}$	$1.5 \cdot 10^{-3}$	$5.9 \cdot 10^{-3}$	$1.5 \cdot 10^{-2}$	$1.8 \cdot 10^{-2}$	$2.0 \cdot 10^{-2}$

Therein, $\mathbf{X} \in \mathbb{R}^{n_x \times N}$ is the scaled test snapshot matrix, having the snapshots $\mathbf{x}^{(k)}$, $k = 1, \dots, N$, as matrix rows. The matrix $\mathbf{X}_r \in \mathbb{R}^{n_x \times N}$ collects the projected or predicted snapshots, $\mathbf{x}_r^{(k)} \in \mathbb{R}^{n_x}$, $k = 1, \dots, N$. We scale and shift \mathbf{X} and \mathbf{X}_r consistently with the training data.

We note, however, that the choice of the error norm and test data set can have a significant impact on the conclusions and should always be selected based on the ROM application. For example, the RMSE averages out peak deviations so that the slow and steady-state errors are prioritized over maximum errors, e.g., an IR on a short-term scale does not drastically increase the error. Herein, our test data set comprises a significant share of slow response and near-stationary snapshots. We consider this choice to be suitable for examining ROMs that capture the slow manifold.

Finally, we describe how the projections for test 1 are obtained. Regarding the linear basis methods POD and DMDc, both the linear subspaces and the projections coincide, respectively. The projection is given by the projection matrix, $\mathbf{\Pi} \triangleq \mathbf{U}_1 \mathbf{U}_1^T$, where \mathbf{U}_1 is from Eq. (10) or Eq. (24). To compute the projections performed by MFL, MFLu, KW, and MFL-ANN, we encode and decode the test data through the respective AENs. The projections in POD-Res, COMP and AGG are inherently defined through the degeneration/residualization. We evaluate these projections by solving the respective nonlinear systems of equations, Eqs. (13b), (16b) and (27b), on the test data in **Dymola**. Recall that for the selected hyperparameters, the slow manifolds of AGG and COMP coincide; however, the projections differ.

5.5. Results: Projection accuracy

We present the results of the projection test. Table 2 compares the projection errors (RMSE) on the test data set. First, we consider small $n_z \leq 10$, i.e., the very-low-order region. As expected, the non-intrusive nonlinear subspace methods (POD-Res, MFL, MFLu) perform significantly better than the linear basis methods (POD, DMDc). The respective difference in RMSE is approximately one order of magnitude. Overall, the smallest projection errors are reached by the MFLu approach. However, the difference in RMSE between MFL and MFLu decreases with increasing n_z . This confirms the limitations of MFL discussed in Section 3.1.5. Clearly, the error difference is system-dependent and may be even more substantial for a strongly parameterized slow manifold. Finally, the projection RMSE of the non-intrusive nonlinear subspace methods KW and MFL-ANN is comparable to POD. The higher RMSE than for MFL is attributed to the additional loss terms included in the KW and MFL-ANN trainings.

Moving to higher orders, i.e., $n_z \in \{16, 28\}$, the improvement by the MFL-based methods is only moderate, which was also observed in [36, 101]. We attribute this limited improvement to the challenging convergence of the respective unsupervised learning problems using local solvers, i.e., training AENs by stochastic gradient descent algorithms. As a result, POD truncation outperforms the MFL methods at $n_z = 28$, facilitating the overall smallest projection error. Interestingly, the linear POD subspace projection also exceeds the accuracy of the nonlinear POD-Res method. A further investigation of the POD-Res results revealed moderate deviations between $\mathbf{x}(t)$ and $\mathbf{x}_r(t)$ at the points of abrupt

Table 3: Results of ROM predictions. The RMSE indicates the average error between the state predictions by the ROMs versus the true FOM states. We consider different ROM orders n_z . Non-converged simulations are indicated by (*).

n_z	POD	DMDc	POD-Res	MFL	MFLu	KW	MFL-ANN	COMP	AGG
2	$1.1 \cdot 10^{-1}$	$1.5 \cdot 10^{-1}$	$3.6 \cdot 10^{-2}$	$6.1 \cdot 10^{-1}$	$2.9 \cdot 10^{-1}$	$1.5 \cdot 10^{-1}$	$1.7 \cdot 10^{-1}$	—	—
5	$6.3 \cdot 10^{-2}$	$1.5 \cdot 10^{-1}$	$2.1 \cdot 10^{-2}$	$1.4 \cdot 10^{-1}$	$2.2 \cdot 10^{-2}$	$1.5 \cdot 10^{-2}$	$2.9 \cdot 10^{-2}$	—	—
10	$4.9 \cdot 10^{-2}$	$1.3 \cdot 10^{-1}$	$8.8 \cdot 10^{-3}$	$2.1 \cdot 10^{-2}$	$1.5 \cdot 10^{-2}$	$9.9 \cdot 10^{-3}$	$3.3 \cdot 10^{-2}$	—	—
16	(*)	$9.4 \cdot 10^{-2}$	$7.9 \cdot 10^{-3}$	$1.0 \cdot 10^{-2}$	$1.1 \cdot 10^{-2}$	$1.9 \cdot 10^{-2}$	$3.2 \cdot 10^{-2}$	$2.5 \cdot 10^{-1}$	$4.9 \cdot 10^{-2}$
28	$8.7 \cdot 10^{-3}$	$7.8 \cdot 10^{-2}$	$7.5 \cdot 10^{-3}$	(*)	(*)	$1.1 \cdot 10^{-2}$	$3.3 \cdot 10^{-2}$	$3.7 \cdot 10^{-2}$	$1.7 \cdot 10^{-2}$

changes in $\mathbf{u}(t)$. Finally, both COMP and AGG exhibit relatively large errors compared to the other ROM methods. Here, the COMP subspace shows significant deviations from the FOM samples near the input steps but relatively small errors otherwise. In contrast, the maximum deviations of AGG are lower, but a greater number of samples have a notable projection error.

5.6. Results: ROM predictions

We now present the results of the ROM prediction test. Table 3 collects the state prediction error (RMSE) of the ROMs. The RMSE is consistently higher than in Table 2, because ROM predictions are less accurate than the (orthogonal) projection of FOM snapshots onto the ROM subspace.

Both linear subspace methods, POD-Galerkin and DMDc, do not reach the desired accuracy at very low order, i.e., $n_z \leq 10$. For reduced orders $11 \leq n_z \leq 21$, the simulations of the POD-Galerkin ROMs did not converge at all. As we discuss in the SI, these critical values of n_z lie below the truncation threshold of $n_z = 23$, obtained from the POD singular values. At order $n_z = 28$, the POD-Galerkin ROM successfully provides an accurate prediction, whereas the DMDc prediction is still poor. Clearly, the nonlinearity of the FOM prohibits highly accurate DMDc models. Finally, we notice a significant gap between projection error (Table 2) and prediction error (Table 3) for both POD-Galerkin and DMDc.

Compared to the POD-Galerkin results, the POD-Res model is more accurate throughout all orders. This advantage is particularly significant in the very-low-order region. In contrast to the projection accuracy (Table 2), POD-Res outperforms the POD-Galerkin ROMs in the prediction. Even for $n_z = 2$, we notice a fairly small prediction error of POD-Res. Since an RMSE of 10^{-2} roughly corresponds to 1% average error in the scaled states, we expect a satisfactory performance of POD-Res ROMs of order $n_z = 10$ (and possibly even $n_z = 5$) in many applications. When moving to higher n_z , the accuracy improves further.

Similarly to POD-Res, the methods MFL and MFLu enable a higher precision than the linear basis methods at very low order (except for $n_z = 2$). Moreover, at $n_z = 5$, the MFLu-Galerkin ROM clearly outperforms the MFL-Galerkin ROM. On the other hand, at higher order, both models perform similarly. At $n_z = 28$, the simulation of both MFL and MFLu ROMs did not converge. Using a different activation function or adding neurons to the AENs did not resolve this issue. A possible cause is the combination of relatively high ROM order at moderate AEN accuracy (similarly to the issues with POD-Galerkin ROMs). Although we are confident that modifications based on more extensive training might facilitate convergence, we did not undertake such attempts. Instead, we highlight the potential numerical issues with higher-order MFL-Galerkin ROMs when working in a standard AEN training setup.

The non-intrusive KW and MFL-ANN ROMs have a prediction error comparable to the intrusive nonlinear subspace methods. The differences in RMSE lie within the range of deviations found in ML trainings. Notably, the MFL-ANN models do not perform better than the KW models. A comparison

to the performance on the training data set revealed a tendency of MFL-ANN to overfit the training data (the RMSEs on the training data were approximately one order of magnitude smaller than on the test data), which was less pronounced for the KW structure. From $n_z = 10$ to $n_z = 28$, there is no improvement in RMSE for both model types, i.e., increasing the ROM order does not improve the accuracy. Finally, we notice that the projection and prediction errors are comparable for both models, respectively.

For COMP and AGG models with a single compartment and aggregation cell for each unit operation, respectively, we find significant prediction errors. In particular, the COMP model is far from the desired accuracy due to severe IR. Increasing the ROM order results in a notably smaller RMSE, where the AGG results reach the desired error level. However, the COMP response still exhibits a notable IR, diminishing ROM accuracy (see figure below).

Besides comparing the numerical results, we also comment on the numerical properties of the ROMs. Performing the simulations was most straightforward using the non-intrusive ROMs (DMDc, KW, MFL-ANN), which are numerically favorable to deal with due to the sequential model structure. On the other hand, simulating the POD-Res and COMP models was computationally most expensive, and required a very careful initialization and scaling of the model equations to converge the simulations. As a result, the high accuracy of the POD-Res model is offset by the fact that it is difficult to handle numerically.

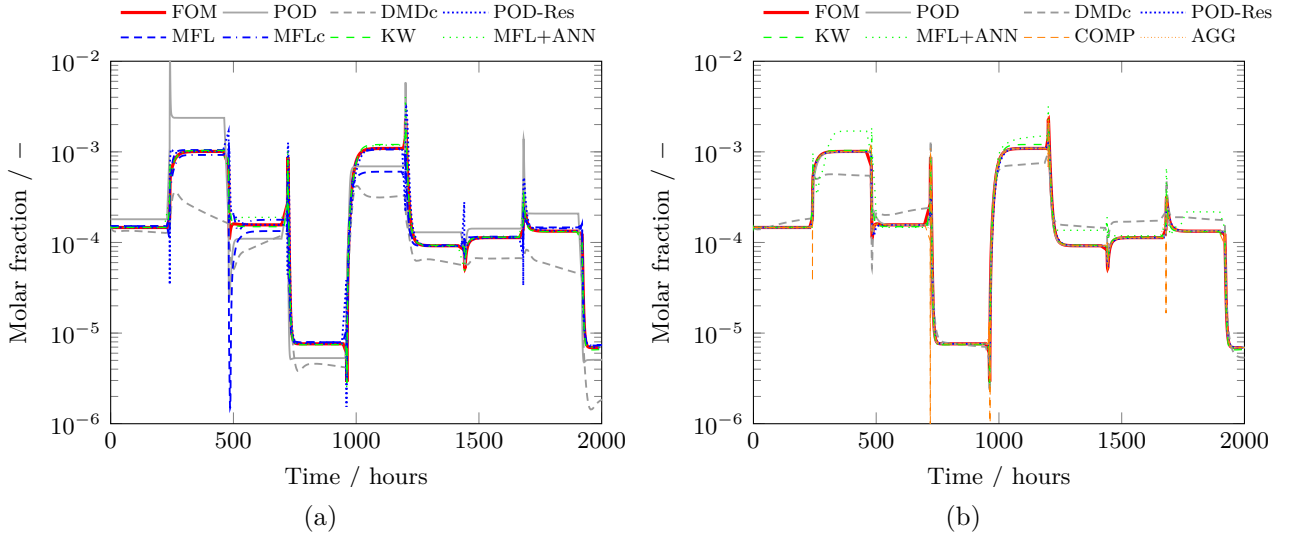


Fig. 5: Results of test 2 (prediction). Depicted is the liquid molar fraction of oxygen on the HPC top stage over the first 2000 h of the test. ROM order is (a) $n_z = 5$ and (b) $n_z = 28$.

To illustrate the results, we examine the molar fraction of oxygen on the HPC top tray, which is directly connected to the quality of the nitrogen product. We show the predictions for $n_z = 5$ in Fig. 5a and for $n_z = 28$ in Fig. 5b. In Fig. 5a, we observe a significant offset between ROM prediction and FOM response for POD, DMDc, and MFL. This finding is consistent with Table 3. For these ROMs, the offset involves both a transient and a steady-state mismatch. Moreover, despite the relatively small RMSE of POD-Res, the graph shows significant IR near the input steps, whereas the steady states are captured accurately. All other ROMs (MFLu, KW, MFL-ANN) reproduce the FOM trajectory closely.

Observing the higher-order case in Fig. 5b, we find significantly better predictions by the POD and POD-Res models. At the same time, the DMDc forecast remains inaccurate. The effect of overfitting discussed above for the MFL-ANN ROMs is also visible in the figure. Compared to Fig. 5a, the prediction is less accurate despite a higher-order model. Further, notable deviations from the FOM trajectory are visible for the COMP model in the form of severe IR. In contrast, the AGG ROM provides a close reproduction of the FOM trajectory.

6. Discussion

Based on theoretical properties of the MOR methods and the findings of the case study, we summarize characteristic properties of the methods investigated. However, we emphasize that definitive statements on a method ranking are delicate, because in addition to n_z , most MOR techniques possess further hyperparameters that can strongly affect ROM behavior, e.g., the position of the sensitive element (COMP, AGG) or the ANN architecture (MFL, KW, MFL-ANN). Although we performed a basic validation of crucial hyperparameters within the case study, we do not claim that this screening was exhaustive. Additionally, the performance of a certain type of ROM may be system-dependent, and in that sense our experimental results may be specific to air separation.

Comparing the results of intrusive (MFL, MFLu) to non-intrusive nonlinear subspace methods (KW, MFL-ANN) in the case study, we conclude that similar ROM accuracies are reached when targeting very low-order models. Such very-low-order ROMs are important in control applications, where CPU reduction has a high priority whereas moderate errors are acceptable. Often, a moderate prediction error can be compensated by state estimation and model adaptation, especially if the error is predominantly steady-state offset [243]. On the other hand, despite a relatively low RMSE, the POD-Res results exhibited an IR in the very-low-order setup, which can be problematic in control applications.

When prioritizing accuracy over low order, non-intrusive methods may struggle to reach arbitrary precision due to their inherently difficult learning problems. In such cases, intrusive strategies can be more easy to apply. In particular, the POD-based methods were able to generate very accurate ROMs given a sufficiently high order. In this context, we acknowledge the simplicity and approximation guarantees (on the training data) of the POD. In contrast, high projection and prediction accuracies were difficult to reach when using MFL strategies.

The advantage of non-intrusive over intrusive reduction methods is that non-intrusive strategies combine MOR and hyperreduction. The weakness of non-intrusive methods is that they can be prone to overfitting if not carefully regularized. One possible “structural regularization” strategy is to restrict the latent dynamics to a linear or bilinear form. In particular, applied Koopman theory combines MFL and linearization into a KW structure, which enables reliable ROMs of the moderately nonlinear systems.

POD-Res and COMP may be considered as data-driven and heuristic variants of SPT, respectively. However, COMP retains most of the model sparsity, whereas POD-Res ROMs are generally dense and can therefore be more challenging to solve. Here, both POD-Res and COMP were numerically the most delicate to handle. Specifically, large-scale implicit nonlinear systems of equations and non-physical IR made these models difficult to converge.

In terms of reduction effort, the (non-intrusive) KW and MFL-ANN strategies involved the most extensive offline computations. Achieving highly accurate models may require multiple trainings and extensive hyperparameter tuning, which introduces delays into the model reduction procedure. Furthermore, non-intrusive methods are most sensible to the training data in our experience. In particular, a balanced amount of transient and stationary data is essential for the successful generation of ROMs that enable precise long-term forecasts.

The model reduction efforts in intrusive reduction methods (including tailored methods) demand a great share of model building and reformulation (debugging, robustification). On the other hand, the ML problems used within intrusive methods, e.g., AEN training, are typically less computationally demanding than in non-intrusive approaches. In our experience, intrusive data-driven methods are slightly more tolerant to a poorly designed data set, e.g., too few steady-state data. For intrusive methods, further efforts have to be expected in terms of hyperreduction, often necessary to obtain a real-time capable ROM.

Lastly, we comment on the model reduction procedure for interconnected systems. Applying the tailored methods, such as COMP and AGG, is naturally done in a “subsystem-by-subsystem” fashion, since these methods provide reduced models of the subsystems, e.g., distillation columns or HXs, of an interconnected system, e.g., a process flowsheet model. In particular, when working in a structured modeling environment, such as **Unisim Design** or **gPROMS**, these ROMs can be pre-configured and included into the model library. Reducing an interconnected system model is then achieved by substituting full-order submodels by reduced submodels. The “subsystem-by-subsystem” approach preserves the model sparsity originating from the interconnection, but the feasible degree of reduction may be limited, as shown by the case study results. Further, the reduction problem becomes a combinatorial problem due to potentially many subsystem ROMs to be configured and combined.

In contrast to the “subsystem-by-subsystem” approach, general-purpose methods are most easily applied to the entire FOM. Then, the complete model of the interconnected system is reduced as a whole. As shown by the case study, such an approach can enable a lower ROM order. However, for systems with many inputs, the data sampling efforts grow exponentially with n_u , which can result in a curse of dimensionality. This curse may be broken by a “subsystem-by-subsystem” strategy if the high-dimensional inputs enter the system only locally and are evenly distributed over the submodels.

7. Conclusions and outlook

Model order reduction spans a collection of techniques to construct a low-order model approximating the evolution of a high-order system. Herein, we have reviewed and compared reduction methods for nonlinear dynamical models with inputs. In particular, we have contrasted the different strategies both theoretically and in a case study. As expected, there is not universal best choice when selecting a reduction method. Rather, a suitable choice depends on targeted ROM properties.

If very-low-order ROMs are needed, then intrusive nonlinear subspace methods, e.g., the MFLu approach, as well as non-intrusive nonlinear subspace methods, e.g., the KW model, have provided accurate ROMs within our case study. Notably, non-intrusive reduction methods combine MOR and hyperreduction in a single step, providing a ROM that is real-time capable. If a high ROM accuracy is needed but the degree of reduction is of secondary importance, then linear subspace methods, e.g., the POD-Galerkin method, are a good choice due to their (theoretically) arbitrary degree of accuracy and simplicity of application. Finally, when desiring structural preservation of a given (network or flowsheet) model comprising interconnected subsystems, then problem-specific ROMs are a straightforward choice to reduce the subunits individually by means of pre-configured ROM blocks.

Besides reviewing and comparing existing MOR methods, we have also proposed an extension of the manifold-Galerkin method to systems with inputs (Section 3.1.5). In particular, we stress that system inputs $\mathbf{u}(t)$ can deform the slow manifold $\mathcal{M}_{\mathcal{X}}$. Consequently, if the effect of inputs is disregarded, an accurate approximation of $\mathcal{M}_{\mathcal{X}}$ may necessitate a higher ROM order. Within the case study, we validated this extension and found that our approach outperforms the state-of-the-art manifold-Galerkin method in cases of very strong reduction both in terms of the projection accuracy and the ROM prediction accuracy. As expected, our extended approach and the established approach performed similarly at higher orders.

In our case study, we did not investigate hyperreduction or CPU cost of integration. Instead, we expect that a sufficiently low order combined with hyperreduction enables real-time applications, e.g., [183, 120]. Clearly, real-time capability depends on the application, so there is no universal CPU threshold to classify performance. In any case, accounting for hyperreduction already within MOR could be a promising step towards more holistic methods.

Despite increasing computer power, nonlinear MOR (especially for parametric and non-autonomous systems) remains a challenging discipline worth of investigation. The curse of dimensionality, when

sampling systems with many inputs or parameters, is connected to the need for robust methods applicable in the low-data limit. In this regard, methods such as physics-informed strategies [244, 104] are a promising approach to enrich the non-intrusive manifold learning task by additional (possibly intrusive) information. Moreover, applying manifold learning methods to very-high-order problems remains an open challenge.

Unfortunately, there are no general guarantees for the preservation of stability properties by MOR methods [34]. Consequently, a-posteriori error and stability analysis are currently required when conducting model reduction. Hence, methods with a-priori error estimates or even guarantees are needed. Despite some recent advances towards modal closure and memory effects, e.g., using the Mori-Zwanzig formalism [245], these works are at an early stage [246].

Finally, we notice some limitations of current reduction methods with respect to numerical optimization and control applications. First, most numerical optimization techniques are based on derivative information, in particular, the Jacobian of the ROM variables $\mathbf{z}(t)$ and $\mathbf{x}_r(t)$ in Eq. (4) with respect to each other and the inputs $\mathbf{u}(t)$. However, standard MOR methods do not explicitly account for the accuracy of such derivatives. For learning-based MOR and hyperreduction approaches, Sobolev trainings [247, 248] may improve derivative accuracy. Additionally, in our experience, sensitivity integration is often considerably more expensive than standard integration, and therefore accounting for sensitivities in the reduction process might enable fundamental improvements in CPU costs of optimization applications. Second, model reduction of non-smooth or even discontinuous models is interesting, e.g., for controlling a process start-up, but remains a mostly unexplored topic [249, 250].

Acknowledgments

We thank Danimir Donecovic and Eike Cramer for fruitful discussions.

References

- [1] W. L. Luyben, *Chemical reactor design and control*. John Wiley & Sons, 2007.
- [2] C. C. Pantelides and J. G. Renfro, “The online use of first-principles models in process operations: Review, current status and future needs,” *Computers & Chemical Engineering*, vol. 51, pp. 136–148, 2013.
- [3] R. Kender, F. Kaufmann, F. Rößler, B. Wunderlich, D. Golubev, I. Thomas, A.-M. Ecker, S. Rehfeldt, and H. Klein, “Development of a digital twin for a flexible air separation unit using a pressure-driven simulation approach,” *Computers & Chemical Engineering*, vol. 151, p. 107349, 2021.
- [4] K. E. Brenan, S. L. Campbell, and L. R. Petzold, *Numerical solution of initial-value problems in differential-algebraic equations*. Siam, 1995.
- [5] W. Marquardt, “Nonlinear model reduction for optimization based control of transient chemical processes,” *AIChE Symposium Series*, 2002.
- [6] A. C. Antoulas, “An overview of approximation methods for large-scale dynamical systems,” *Annual Reviews in Control*, vol. 29, no. 2, pp. 181–190, 2005.
- [7] C. W. Rowley and S. T. Dawson, “Model Reduction for Flow Analysis and Control,” *Annual Review of Fluid Mechanics*, vol. 49, no. 1, pp. 387–417, 2017.
- [8] K. T. Wong and R. Luus, “Model reduction of high-order multistage systems by the method of orthogonal collocation,” *The Canadian Journal of Chemical Engineering*, vol. 58, no. 3, pp. 382–388, 1980.

- [9] P. Haider, P. Freko, T. Acher, S. Rehfeldt, and H. Klein, “A transient three-dimensional model for thermo-fluid simulation of cryogenic plate-fin heat exchangers,” *Applied Thermal Engineering*, vol. 180, p. 115791, 2020.
- [10] C. Georgakis, R. Aris, and N. R. Amundson, “Studies in the control of tubular reactors-I General Considerations,” *Chemical Engineering Science*, vol. 32, no. 11, pp. 1359–1369, 1977.
- [11] P. Daoutidis, “DAEs in model reduction of chemical processes: An overview,” in *Surveys in Differential-Algebraic Equations II*, pp. 69–102, Springer, 2015.
- [12] B. E. Okeke and Roussel, “An invariant-manifold approach to lumping,” *Mathematical Modelling of Natural Phenomena*, vol. 10, no. 3, pp. 149–167, 2015.
- [13] M. D. Graham and I. G. Kevrekidis, “Alternative approaches to the Karhunen-Loeve decomposition for model reduction and data analysis,” *Computers & Chemical Engineering*, vol. 20, no. 5, pp. 495–506, 1996.
- [14] A. J. Roberts, “The Utility of an Invariant Manifold Description of the Evolution of a Dynamical System,” *SIAM Journal on Mathematical Analysis*, vol. 20, no. 6, pp. 1447–1458, 1989.
- [15] H. Nijmeijer and A. van der Schaft, *Nonlinear Dynamical Control Systems*. New York, NY: Springer New York, 1990.
- [16] L. Horstmeyer and F. M. Atay, “Characterization of exact lumpability for vector fields on smooth manifolds,” *Differential Geometry and its Applications*, vol. 48, pp. 46–60, 2016.
- [17] S. Y. Shvartsman and I. G. Kevrekidis, “Nonlinear model reduction for control of distributed systems: A computer-assisted study,” *AIChE Journal*, vol. 44, no. 7, pp. 1579–1595, 1998.
- [18] U. Baur, P. Benner, and L. Feng, “Model order reduction for linear and nonlinear systems: a system-theoretic perspective,” *Archives of Computational Methods in Engineering*, vol. 21, no. 4, pp. 331–358, 2014.
- [19] P. J. Schmid, “Dynamic mode decomposition of numerical and experimental data,” *Journal of fluid mechanics*, vol. 656, pp. 5–28, 2010.
- [20] A. C. Antoulas, *Approximation of large-scale dynamical systems*. Siam, 2005.
- [21] G. Rozza, G. Stabile, and F. Ballarin, eds., *Advanced Reduced Order Methods and Applications in Computational Fluid Dynamics*. Philadelphia, PA: Society for Industrial and Applied Mathematics, 2022.
- [22] M. Rathinam and L. R. Petzold, “A New Look at Proper Orthogonal Decomposition,” *SIAM Journal on Numerical Analysis*, vol. 41, no. 5, pp. 1893–1925, 2003.
- [23] M. Ohlberger and S. Rave, “Reduced basis methods: Success, limitations and future challenges,” *Proceedings Of The Conference Algoritmy*, pp. 1–12, 2016.
- [24] G. Berkooz, P. Holmes, and J. L. Lumley, “The proper orthogonal decomposition in the analysis of turbulent flows,” *Annual Review of Fluid Mechanics*, vol. 25, no. 1, pp. 539–575, 1993.
- [25] B. Moore, “Principal component analysis in linear systems: Controllability, observability, and model reduction,” *IEEE Transaction on automatic control*, vol. 26, no. 1, pp. 17–32, 1981.
- [26] J. Hahn and T. F. Edgar, “An improved method for nonlinear model reduction using balancing of empirical gramians,” *Computers & Chemical Engineering*, vol. 26, no. 10, pp. 1379–1397, 2002.
- [27] H. K. Khalil, “Nonlinear systems third edition,” *Patience Hall*, vol. 115, 2002.

[28] R. Romijn, *Empirical model reduction of differential-algebraic equation systems*. Dissertation, RWTH Aachen University, 2016.

[29] J. R. Phillips, “Projection-based approaches for model reduction of weakly nonlinear, time-varying systems,” *IEEE Transactions on Computer-Aided Design of Integrated Circuits and Systems*, vol. 22, no. 2, pp. 171–187, 2003.

[30] L. Feng, X. Zeng, C. Chiang, D. Zhou, and Q. Fang, “Direct nonlinear order reduction with variational analysis,” in *Proceedings Design, Automation and Test in Europe Conference and Exhibition*, pp. 1316–1321, IEEE Comput. Soc, 2004.

[31] C. Gu, “QLMOR: A Projection-Based Nonlinear Model Order Reduction Approach Using Quadratic-Linear Representation of Nonlinear Systems,” *IEEE Transactions on Computer-Aided Design of Integrated Circuits and Systems*, vol. 30, no. 9, pp. 1307–1320, 2011.

[32] I. Mezić, “Spectral properties of dynamical systems, model reduction and decompositions,” *Nonlinear Dynamics*, vol. 41, no. 1, pp. 309–325, 2005.

[33] M. O. Williams, I. G. Kevrekidis, and C. W. Rowley, “A data–driven approximation of the koopman operator: Extending dynamic mode decomposition,” *Journal of Nonlinear Science*, vol. 25, no. 6, pp. 1307–1346, 2015.

[34] J. S. Hesthaven, C. Pagliantini, and G. Rozza, “Reduced basis methods for time-dependent problems,” *Acta Numerica*, vol. 31, pp. 265–345, 2022.

[35] F. Jauberteau, C. Rosier, and R. Temam, “The nonlinear Galerkin method in computational fluid dynamics,” *Applied Numerical Mathematics*, vol. 6, no. 5, pp. 361–370, 1990.

[36] K. Lee and K. T. Carlberg, “Model reduction of dynamical systems on nonlinear manifolds using deep convolutional autoencoders,” *Journal of Computational Physics*, vol. 404, p. 108973, 2020.

[37] J. Hahn, S. Lextrait, and T. F. Edgar, “Nonlinear balanced model residualization via neural networks,” *AICHE Journal*, vol. 48, no. 6, pp. 1353–1357, 2002.

[38] D. Ryckelynck, “Hyper-reduction of mechanical models involving internal variables,” *International Journal for Numerical Methods in Engineering*, vol. 77, no. 1, pp. 75–89, 2009.

[39] M. Barrault, Y. Maday, N. C. Nguyen, and A. T. Patera, “An ‘empirical interpolation’ method: application to efficient reduced-basis discretization of partial differential equations,” *Comptes Rendus. Mathématique*, vol. 339, no. 9, pp. 667–672, 2004.

[40] M. Rewieński and J. White, “Model order reduction for nonlinear dynamical systems based on trajectory piecewise-linear approximations,” *Linear algebra and its applications*, vol. 415, no. 2-3, pp. 426–454, 2006.

[41] R. Bos, X. Bombois, and P. van den Hof, “Accelerating large-scale non-linear models for monitoring and control using spatial and temporal correlations,” *Proceedings of the 2004 American Control Conference*, pp. 3705–3710, 2004.

[42] N. C. Nguyen and J. Peraire, “An efficient reduced–order modeling approach for non–linear parametrized partial differential equations,” *International Journal for Numerical Methods in Engineering*, vol. 76, no. 1, pp. 27–55, 2008.

[43] S. Chaturantabut and D. C. Sorensen, “Nonlinear model reduction via discrete empirical interpolation,” *SIAM journal on scientific computing*, vol. 32, no. 5, pp. 2737–2764, 2010.

[44] S. L. Brunton, J. L. Proctor, and J. N. Kutz, “Discovering governing equations from data by sparse identification of nonlinear dynamical systems,” *Proceedings of the National Academy of Sciences*, vol. 113, no. 15, pp. 3932–3937, 2016.

[45] S. Y. Shvartsman, C. Theodoropoulos, R. Rico-Martinez, I. G. Kevrekidis, E. S. Titi, and T. J. Mountziaris, “Order reduction for nonlinear dynamic models of distributed reacting systems,” *Journal of Process Control*, vol. 10, no. 2-3, pp. 177–184, 2000.

[46] U. M. Diwekar, “How simple can it be? — A look at the models for batch distillation,” *Computers & Chemical Engineering*, vol. 18, pp. S451–S457, 1994.

[47] J. D. Hedengren and T. F. Edgar, “Order reduction of large scale DAE models,” *Computers & Chemical Engineering*, vol. 29, no. 10, pp. 2069–2077, 2005.

[48] J. T. Lüthje, J. C. Schulze, A. Caspary, A. Mhamdi, A. Mitsos, and P. Schäfer, “Adaptive Learning of Hybrid Models for Nonlinear Model Predictive Control of Distillation Columns,” *IFAC-PapersOnLine*, vol. 54, no. 3, pp. 37–42, 2021.

[49] M.-Y. L. Lee, “Estimation of the error in the reduced basis method solution of differential algebraic equation systems,” *SIAM Journal on Numerical Analysis*, vol. 28, no. 2, pp. 512–528, 1991.

[50] C. Sun and J. Hahn, “Reduction of stable differential–algebraic equation systems via projections and system identification,” *Journal of Process Control*, vol. 15, no. 6, pp. 639–650, 2005.

[51] J. C. Schulze, D. T. Oncevic, and A. Mitsos, “Identification of MIMO Wiener-type Koopman models for data-driven model reduction using deep learning,” *Computers & Chemical Engineering*, vol. 161, no. 15, p. 107781, 2022.

[52] A. Astolfi, “Model reduction by moment matching for linear and nonlinear systems,” *IEEE Transaction on automatic control*, vol. 55, no. 10, pp. 2321–2336, 2010.

[53] D. Givon, R. Kupferman, and A. Stuart, “Extracting macroscopic dynamics: model problems and algorithms,” *Nonlinearity*, vol. 17, no. 6, pp. R55–R127, 2004.

[54] R. Kumar and D. Ezhilarasi, “A state-of-the-art survey of model order reduction techniques for large-scale coupled dynamical systems,” *International Journal of Dynamics and Control*, vol. 11, no. 2, pp. 900–916, 2023.

[55] S. Mallick and M. Mittal, “AI-Based Model Order Reduction Techniques: A Survey,” *Archives of Computational Methods in Engineering*, pp. 1–26, 2025.

[56] G. Obinata and B. D. O. Anderson, *Model reduction for control system design*. Communications and Control Engineering, London and Berlin and Heidelberg: Springer, 2001.

[57] B. R. Noack, M. Morzynski, and G. Tadmor, *Reduced-order modelling for flow control*, vol. 528. Springer Science & Business Media, 2011.

[58] P. Holmes, *Turbulence, coherent structures, dynamical systems and symmetry*. Cambridge University Press, 2 ed., 2012.

[59] P. Benner, M. Ohlberger, A. Cohen, and K. Willcox, *Model reduction and approximation: theory and algorithms*. Siam, 2017.

[60] M. Schlegel, J. vd Berg, W. Marquardt, and O. H. Bosgra, “Projection based model reduction for dynamic optimization,” in *AICHE Annual Meeting. Indianapolis*, 2002.

[61] J. Hahn, U. Kruger, and T. F. Edgar, “Application of model reduction for model predictive control,” *IFAC Proceedings Volumes*, vol. 35, no. 1, pp. 393–398, 2002.

[62] L. Pernebo and L. Silverman, “Model reduction via balanced state space representations,” *0018-9286*, vol. 27, no. 2, pp. 382–387, 1982.

- [63] J. M. A. Scherpen, “Balancing for nonlinear systems,” *Systems & Control Letters*, vol. 21, no. 2, pp. 143–153, 1993.
- [64] S. Lall, J. E. Marsden, and S. Glavaški, “Empirical model reduction of controlled nonlinear systems,” *IFAC Proceedings Volumes*, vol. 32, no. 2, pp. 2598–2603, 1999.
- [65] C. Himpe and M. Ohlberger, “Cross-gramian-based combined state and parameter reduction for large-scale control systems,” *Mathematical Problems in Engineering*, vol. 2014, 2014.
- [66] G. Scarciotti and A. Astolfi, “Data-driven model reduction by moment matching for linear and nonlinear systems,” *Automatica*, vol. 79, pp. 340–351, 2017.
- [67] F. J. Baader, P. Althaus, A. Bardow, and M. Dahmen, “Demand response for flat nonlinear MIMO processes using dynamic ramping constraints,” *Computers & Chemical Engineering*, vol. 172, p. 108171, 2023.
- [68] J. M. Lee, *Introduction to Smooth Manifolds*, vol. 218. New York, NY: Springer New York, 2012.
- [69] J. R. Munkres, *Analysis on manifolds*. Addison-Wesley Publishing, 1991.
- [70] N. Boumal, *An introduction to optimization on smooth manifolds*. Cambridge University Press, 2023.
- [71] R. Parker, B. Nicholson, J. Siirola, C. Laird, and L. Biegler, “An implicit function formulation for optimization of discretized index-1 differential algebraic systems,” *Computers & Chemical Engineering*, vol. 168, p. 108042, 2022.
- [72] W. C. Rheinboldt, “Differential-algebraic systems as differential equations on manifolds,” *Mathematics of Computation*, vol. 43, no. 168, pp. 473–482, 1984.
- [73] H.-P. Löffler and W. Marquardt, “Order reduction of non-linear differential-algebraic process models,” *Journal of Process Control*, vol. 1, no. 1, pp. 32–40, 1991.
- [74] A. C. Antoulas, D. C. Sorensen, and S. Gugercin, “A survey of model reduction methods for large-scale systems,” *Contemporary mathematics*, vol. 280, pp. 193–220, 2001.
- [75] Z. Bai, “Krylov subspace techniques for reduced-order modeling of large-scale dynamical systems,” *Applied Numerical Mathematics*, vol. 43, no. 1-2, pp. 9–44, 2002.
- [76] A. Chatterjee, “An introduction to the proper orthogonal decomposition,” *Current science*, pp. 808–817, 2000.
- [77] P. Benner, S. Gugercin, and K. Willcox, “A survey of projection-based model reduction methods for parametric dynamical systems,” *SIAM review*, vol. 57, no. 4, pp. 483–531, 2015.
- [78] P. Binev, A. Cohen, W. Dahmen, R. DeVore, G. Petrova, and P. Wojtaszczyk, “Convergence Rates for Greedy Algorithms in Reduced Basis Methods,” *SIAM Journal on Mathematical Analysis*, vol. 43, no. 3, pp. 1457–1472, 2011.
- [79] G. Rozza, D. B. P. Huynh, and A. T. Patera, “Reduced Basis Approximation and a Posteriori Error Estimation for Affinely Parametrized Elliptic Coercive Partial Differential Equations,” *Archives of Computational Methods in Engineering*, vol. 15, no. 3, pp. 229–275, 2008.
- [80] P. V. Kokotovic, R. E. O’Malley Jr, and P. Sannuti, “Singular perturbations and order reduction in control theory—an overview,” *Automatica*, vol. 12, no. 2, pp. 123–132, 1976.
- [81] K. Weischedel and T. J. McAvoy, “Feasibility of decoupling in conventionally controlled distillation columns,” *Industrial & Engineering Chemistry Fundamentals*, vol. 19, no. 4, pp. 379–384, 1980.

[82] B. Roffel, B. H. L. Betlem, and J. A. de Ruijter, “First principles dynamic modeling and multi-variable control of a cryogenic distillation process,” *Computers & Chemical Engineering*, vol. 24, no. 1, pp. 111–123, 2000.

[83] A. Haro, M. Canadell, J.-L. Figueras, A. Luque, and J.-M. Mondelo, “The parameterization method for invariant manifolds,” *Applied mathematical sciences*, vol. 195, 2016.

[84] S. Jain and G. Haller, “How to compute invariant manifolds and their reduced dynamics in high-dimensional finite element models,” *Nonlinear Dynamics*, vol. 107, no. 2, pp. 1417–1450, 2022.

[85] A. Benallou, D. E. Seborg, and D. A. Mellichamp, “Dynamic compartmental models for separation processes,” *AIChE Journal*, vol. 32, no. 7, pp. 1067–1078, 1986.

[86] E. Ranzi, M. Rovaglio, T. Faravelli, and G. Biardi, “Role of energy balances in dynamic simulation of multicomponent distillation columns,” *Computers & Chemical Engineering*, vol. 12, no. 8, pp. 783–786, 1988.

[87] R. R. Horton, B. W. Bequette, and T. F. Edgar, “Improvements in dynamic compartmental modeling for distillation,” *Computers & Chemical Engineering*, vol. 15, no. 3, pp. 197–201, 1991.

[88] C. Foias and R. Temam, “The algebraic approximation of attractors: The finite dimensional case,” *Physica D: Nonlinear Phenomena*, vol. 32, no. 2, pp. 163–182, 1988.

[89] M. Marion and R. Temam, “Nonlinear Galerkin Methods,” *SIAM Journal on Numerical Analysis*, vol. 26, no. 5, pp. 1139–1157, 1989.

[90] N. Mahadevan and K. A. Hoo, “Wavelet-based model reduction of distributed parameter systems,” *Chemical Engineering Science*, vol. 55, no. 19, pp. 4271–4290, 2000.

[91] Y. Ma and Y. Fu, *Manifold Learning Theory and Applications*. CRC press, 2011.

[92] P. Baldi and K. Hornik, “Neural networks and principal component analysis: Learning from examples without local minima,” *Neural networks*, vol. 2, no. 1, pp. 53–58, 1989.

[93] M. A. Kramer, “Autoassociative neural networks,” *Computers & Chemical Engineering*, vol. 16, no. 4, pp. 313–328, 1992.

[94] T. Kohonen, “Self-organized formation of topologically correct feature maps,” *Biol. Cybern.*, vol. 43, no. 1, pp. 59–69, 1982.

[95] B. Schölkopf, A. Smola, and K.-R. Müller, “Kernel principal component analysis,” in *International conference on artificial neural networks*, pp. 583–588, 1997.

[96] S. Mika, B. Schölkopf, A. Smola, K.-R. Müller, M. Scholz, and G. Rätsch, “Kernel PCA and de-noising in feature spaces,” *Advances in Neural Information Processing Systems*, vol. 11, 1998.

[97] S. T. Roweis and L. K. Saul, “Nonlinear dimensionality reduction by locally linear embedding,” *science*, vol. 290, no. 5500, pp. 2323–2326, 2000.

[98] M. Belkin and P. Niyogi, “Laplacian eigenmaps for dimensionality reduction and data representation,” *Neural computation*, vol. 15, no. 6, pp. 1373–1396, 2003.

[99] R. R. Coifman and S. Lafon, “Diffusion maps,” *Applied and Computational Harmonic Analysis*, vol. 21, no. 1, pp. 5–30, 2006.

[100] B. Ghojogh, M. Crowley, F. Karray, and A. Ghodsi, *Elements of Dimensionality Reduction and Manifold Learning*. Cham: Springer International Publishing, 2023.

- [101] T. R. F. Phillips, C. E. Heaney, P. N. Smith, and C. C. Pain, “An autoencoder-based reduced-order model for eigenvalue problems with application to neutron diffusion,” *International Journal for Numerical Methods in Engineering*, vol. 122, no. 15, pp. 3780–3811, 2021.
- [102] P. Vincent, H. Larochelle, Y. Bengio, and P.-A. Manzagol, “Extracting and composing robust features with denoising autoencoders,” in *Proceedings of the 25th international conference on Machine learning*, pp. 1096–1103, 2008.
- [103] K. Kashima, “Nonlinear model reduction by deep autoencoder of noise response data,” *IEEE 55th Conference on Decision and Control (CDC)*, pp. 5750–5755, 2016.
- [104] S. E. Otto, G. R. Macchio, and C. W. Rowley, “Learning nonlinear projections for reduced-order modeling of dynamical systems using constrained autoencoders,” *Chaos: An Interdisciplinary Journal of Nonlinear Science*, vol. 33, no. 11, 2023.
- [105] S. Fresca and A. Manzoni, “POD-DL-ROM: Enhancing deep learning-based reduced order models for nonlinear parametrized PDEs by proper orthogonal decomposition,” *Computer Methods in Applied Mechanics and Engineering*, vol. 388, p. 114181, 2022.
- [106] F. Romor, G. Stabile, and G. Rozza, “Non-linear Manifold Reduced-Order Models with Convolutional Autoencoders and Reduced Over-Collocation Method,” *Journal of Scientific Computing*, vol. 94, no. 3, 2023.
- [107] P. Benner, M. Ohlberger, A. Patera, G. Rozza, and K. Urban, eds., *Model Reduction of Parametrized Systems*. MS&A, Cham: Springer International Publishing, 2017.
- [108] H. V. Ly and H. T. Tran, “Modeling and control of physical processes using proper orthogonal decomposition,” *Mathematical and Computer Modelling*, vol. 33, no. 1-3, pp. 223–236, 2001.
- [109] T. Bui-Thanh, M. Damodaran, and K. Willcox, “Proper orthogonal decomposition extensions for parametric applications in compressible aerodynamics,” in *21st AIAA applied aerodynamics conference*, p. 4213, 2003.
- [110] L. Mainini and K. Willcox, “Surrogate modeling approach to support real-time structural assessment and decision making,” *AIAA journal*, vol. 53, no. 6, pp. 1612–1626, 2015.
- [111] J. S. Hesthaven and S. Ubbiali, “Non-intrusive reduced order modeling of nonlinear problems using neural networks,” *Journal of Computational Physics*, vol. 363, pp. 55–78, 2018.
- [112] T. Franz, R. Zimmermann, S. Götz, and N. Karcher, “Interpolation-based reduced-order modelling for steady transonic flows via manifold learning,” *International Journal of Computational Fluid Dynamics*, vol. 28, no. 3-4, pp. 106–121, 2014.
- [113] P. Díez, A. Muixí, S. Zlotnik, and A. García-González, “Nonlinear dimensionality reduction for parametric problems: A kernel proper orthogonal decomposition,” *International Journal for Numerical Methods in Engineering*, vol. 122, no. 24, pp. 7306–7327, 2021.
- [114] A. Holiday, M. Kooshkbaghi, J. M. Bello-Rivas, C. W. Gear, A. Zagaris, and I. G. Kevrekidis, “Manifold learning for parameter reduction,” *Journal of Computational Physics*, vol. 392, pp. 419–431, 2019.
- [115] S. Klus, F. Nüske, P. Koltai, H. Wu, I. Kevrekidis, C. Schütte, and F. Noé, “Data-driven model reduction and transfer operator approximation,” *Journal of Nonlinear Science*, vol. 28, no. 3, pp. 985–1010, 2018.
- [116] S. L. Brunton, B. R. Noack, and P. Koumoutsakos, “Machine Learning for Fluid Mechanics,” *Annual Review of Fluid Mechanics*, vol. 52, no. 1, pp. 477–508, 2020.

- [117] O. Ghattas and K. Willcox, “Learning physics-based models from data: perspectives from inverse problems and model reduction,” *Acta Numerica*, vol. 30, pp. 445–554, 2021.
- [118] B. Kramer and K. E. Willcox, “Nonlinear model order reduction via lifting transformations and proper orthogonal decomposition,” *AIAA journal*, vol. 57, no. 6, pp. 2297–2307, 2019.
- [119] A. M. Schweidtmann and A. Mitsos, “Deterministic global optimization with artificial neural networks embedded,” *Journal of Optimization Theory and Applications*, vol. 180, no. 3, pp. 925–948, 2019.
- [120] J. C. Schulze, D. T. Donecic, N. Erwes, and A. Mitsos, “Data-Driven Model Reduction and Nonlinear Model Predictive Control of an Air Separation Unit by Applied Koopman Theory,” *Foundations of Computer Aided Process Operations / Chemical Process Control (FOCAPO)*, 2023.
- [121] A. J. Mayo and A. Antoulas, “A framework for the solution of the generalized realization problem,” *Linear algebra and its applications*, vol. 425, no. 2-3, pp. 634–662, 2007.
- [122] B. Peherstorfer, S. Gugercin, and K. Willcox, “Data-Driven Reduced Model Construction with Time-Domain Loewner Models,” *SIAM journal on scientific computing*, vol. 39, no. 5, pp. A2152–A2178, 2017.
- [123] J.-N. Juang and R. S. Pappa, “An eigensystem realization algorithm for modal parameter identification and model reduction,” *Journal of guidance, control, and dynamics*, vol. 8, no. 5, pp. 620–627, 1985.
- [124] J. L. Proctor, S. L. Brunton, and J. N. Kutz, “Dynamic mode decomposition with control,” *SIAM Journal on Applied Dynamical Systems*, vol. 15, no. 1, pp. 142–161, 2016.
- [125] Q. Lu and V. M. Zavala, “Image-based model predictive control via dynamic mode decomposition,” *Journal of Process Control*, vol. 104, pp. 146–157, 2021.
- [126] L. C. Iacob, R. Tóth, and M. Schoukens, “Koopman form of nonlinear systems with inputs,” *Automatica*, vol. 162, p. 111525, 2024.
- [127] S. E. Otto and C. W. Rowley, “Koopman operators for estimation and control of dynamical systems,” *Annual Review of Control, Robotics, and Autonomous Systems*, vol. 4, pp. 59–87, 2021.
- [128] Q. Li, F. Dietrich, E. M. Bollt, and I. G. Kevrekidis, “Extended dynamic mode decomposition with dictionary learning: A data-driven adaptive spectral decomposition of the Koopman operator,” *Chaos: An Interdisciplinary Journal of Nonlinear Science*, vol. 27, no. 10, p. 103111, 2017.
- [129] S. Das and D. Giannakis, “Koopman spectra in reproducing kernel Hilbert spaces,” *Applied and Computational Harmonic Analysis*, vol. 49, no. 2, pp. 573–607, 2020.
- [130] P. Héas, C. Herzet, and B. Combès, “Nonlinear Reduced Modeling of Dynamical Systems Using Kernel Methods and Low-Rank Approximation,” *Journal of Nonlinear Science*, vol. 35, no. 3, 2025.
- [131] F. Köhne, F. M. Philipp, M. Schaller, A. Schiela, and K. Worthmann, “L $^{\infty}$ -error Bounds for Approximations of the Koopman Operator by Kernel Extended Dynamic Mode Decomposition,” *SIAM Journal on Applied Dynamical Systems*, vol. 24, no. 1, pp. 501–529, 2025.
- [132] M. Korda and I. Mezić, “Linear predictors for nonlinear dynamical systems: Koopman operator meets model predictive control,” *Automatica*, vol. 93, no. 1, pp. 149–160, 2018.

- [133] A. Narasingam and J. S.-I. Kwon, “Koopman Lyapunov–based model predictive control of nonlinear chemical process systems,” *AIChE Journal*, vol. 65, no. 11, p. e16743, 2019.
- [134] K. Hara, M. Inoue, and N. Sebe, “Dissipativity-constrained learning of MPC with guaranteeing closed-loop stability,” *Automatica*, vol. 157, p. 111271, 2023.
- [135] W. Hao, B. Huang, W. Pan, Di Wu, and S. Mou, “Deep Koopman learning of nonlinear time-varying systems,” *Automatica*, vol. 159, p. 111372, 2024.
- [136] M. O. Williams, M. S. Hemati, S. T. Dawson, I. G. Kevrekidis, and C. W. Rowley, “Extending Data-Driven Koopman Analysis to Actuated Systems,” *IFAC-PapersOnLine*, vol. 49, no. 18, pp. 704–709, 2016.
- [137] A. Surana, “Koopman operator based observer synthesis for control-affine nonlinear systems,” *2016 IEEE 55th Conference on Decision and Control (CDC)*, pp. 6492–6499, 2016.
- [138] S. Peitz, S. E. Otto, and C. W. Rowley, “Data-driven model predictive control using interpolated Koopman generators,” *SIAM Journal on Applied Dynamical Systems*, vol. 19, no. 3, pp. 2162–2193, 2020.
- [139] S. E. Otto and C. W. Rowley, “Linearly Recurrent Autoencoder Networks for Learning Dynamics,” *SIAM Journal on Applied Dynamical Systems*, vol. 18, no. 1, pp. 558–593, 2019.
- [140] S. Peitz and S. Klus, “Koopman operator-based model reduction for switched-system control of PDEs,” *Automatica*, vol. 106, pp. 184–191, 2019.
- [141] B. Lusch, J. N. Kutz, and S. Brunton, “Deep learning for universal linear embeddings of nonlinear dynamics,” *Nature Communications*, vol. 9, no. 1, pp. 1–10, 2018.
- [142] J. C. Schulze and A. Mitsos, “Data-driven Nonlinear Model Reduction using Koopman Theory: Integrated Control Form and NMPC Case Study,” *IEEE Control Systems Letters (L-CSS)*, vol. 6, pp. 2978–2983, 2022.
- [143] M. Korda and I. Mezić, “Optimal construction of Koopman eigenfunctions for prediction and control,” *IEEE Transaction on automatic control*, vol. 65, no. 12, pp. 5114–5129, 2020.
- [144] W.-H. Steeb and F. Wilhelm, “Non-linear autonomous systems of differential equations and Carleman linearization procedure,” *Journal of Mathematical Analysis and Applications*, vol. 77, no. 2, pp. 601–611, 1980.
- [145] M. Rewienski and J. White, “A trajectory piecewise-linear approach to model order reduction and fast simulation of nonlinear circuits and micromachined devices,” *IEEE Transactions on Computer-Aided Design of Integrated Circuits and Systems*, vol. 22, no. 2, pp. 155–170, 2003.
- [146] E. Qian, B. Kramer, B. Peherstorfer, and K. Willcox, “Lift & Learn: Physics-informed machine learning for large-scale nonlinear dynamical systems,” *Physica D: Nonlinear Phenomena*, vol. 406, p. 132401, 2020.
- [147] B. Peherstorfer and K. Willcox, “Data-driven operator inference for nonintrusive projection-based model reduction,” *Computer Methods in Applied Mechanics and Engineering*, vol. 306, pp. 196–215, 2016.
- [148] R. Geelen, S. Wright, and K. Willcox, “Operator inference for non-intrusive model reduction with quadratic manifolds,” *Computer Methods in Applied Mechanics and Engineering*, vol. 403, p. 115717, 2023.
- [149] Z. Wang, D. Xiao, F. Fang, R. Govindan, C. C. Pain, and Y. Guo, “Model identification of reduced order fluid dynamics systems using deep learning,” *International Journal for Numerical Methods in Fluids*, vol. 86, no. 4, pp. 255–268, 2018.

[150] P. Wu, J. Sun, X. Chang, W. Zhang, R. Arcucci, Y. Guo, and C. C. Pain, “Data-driven reduced order model with temporal convolutional neural network,” *Computer Methods in Applied Mechanics and Engineering*, vol. 360, p. 112766, 2020.

[151] H. Gao, J.-X. Wang, and M. J. Zahr, “Non-intrusive model reduction of large-scale, nonlinear dynamical systems using deep learning,” *Physica D: Nonlinear Phenomena*, vol. 412, p. 132614, 2020.

[152] S. Wiewel, M. Becher, and N. Thuerey, “Latent space physics: Towards learning the temporal evolution of fluid flow,” in *Computer graphics forum*, vol. 38, pp. 71–82, 2019.

[153] C. Tsay and M. Baldea, “Integrating production scheduling and process control using latent variable dynamic models,” *Control Engineering Practice*, vol. 94, p. 104201, 2020.

[154] S. E. Otto, A. Padovan, and C. W. Rowley, “Optimizing Oblique Projections for Nonlinear Systems using Trajectories,” *SIAM journal on scientific computing*, vol. 44, no. 3, pp. A1681–A1702, 2022.

[155] M. Watter, J. Springenberg, J. Boedecker, and M. Riedmiller, “Embed to control: A locally linear latent dynamics model for control from raw images,” *Advances in Neural Information Processing Systems*, vol. 28, 2015.

[156] R. Goroshin, M. F. Mathieu, and Y. LeCun, “Learning to linearize under uncertainty,” *Advances in Neural Information Processing Systems*, vol. 28, 2015.

[157] F. J. Gonzalez and M. Balajewicz, “Deep convolutional recurrent autoencoders for learning low-dimensional feature dynamics of fluid systems,” *arXiv*, 2018.

[158] J.-A. M. Assael, N. Wahlström, T. B. Schön, and M. P. Deisenroth, “Data-efficient learning of feedback policies from image pixels using deep dynamical models,” *arXiv preprint arXiv:1510.02173*, 2015.

[159] D. Masti and A. Bemporad, “Learning nonlinear state–space models using autoencoders,” *Automatica*, vol. 129, p. 109666, 2021.

[160] S. Fresca, L. Dede’, and A. Manzoni, “A comprehensive deep learning-based approach to reduced order modeling of nonlinear time-dependent parametrized PDEs,” *Journal of Scientific Computing*, vol. 87, pp. 1–36, 2021.

[161] P. Conti, G. Gobat, S. Fresca, A. Manzoni, and A. Frangi, “Reduced order modeling of parametrized systems through autoencoders and SINDy approach: continuation of periodic solutions,” *Computer Methods in Applied Mechanics and Engineering*, vol. 411, p. 116072, 2023.

[162] K. Willcox and J. Peraire, “Balanced model reduction via the proper orthogonal decomposition,” *AIAA journal*, vol. 40, no. 11, pp. 2323–2330, 2002.

[163] R. K. Pearson, “Selecting nonlinear model structures for computer control,” *Journal of Process Control*, vol. 13, no. 1, pp. 1–26, 2003.

[164] B. Besselink, N. van de Wouw, and H. Nijmeijer, “Model reduction for nonlinear systems with incremental gain or passivity properties,” *Automatica*, vol. 49, no. 4, pp. 861–872, 2013.

[165] M. F. Shakib, G. Scarciotti, A. Y. Pogromsky, A. Pavlov, and N. van de Wouw, “Model reduction by moment matching with preservation of global stability for a class of nonlinear models,” *Automatica*, vol. 157, p. 111227, 2023.

[166] E. Esche, D. Müller, R. Kraus, and G. Wozny, “Systematic approaches for model derivation for optimization purposes,” *Chemical Engineering Science*, vol. 115, pp. 215–224, 2014.

[167] N. Jourdan, T. Neveux, O. Potier, M. Kanniche, J. Wicks, I. Nopens, U. Rehman, and Y. Le Moullec, “Compartmental Modelling in chemical engineering: A critical review,” *Chemical Engineering Science*, vol. 210, p. 115196, 2019.

[168] J. Lévine and P. Rouchon, “Quality control of binary distillation columns via nonlinear aggregated models,” *Automatica*, vol. 27, no. 3, pp. 463–480, 1991.

[169] A. Linhart and S. Skogestad, “Reduced distillation models via stage aggregation,” *Chemical Engineering Science*, vol. 65, no. 11, pp. 3439–3456, 2010.

[170] E. Hairer, S. P. Norsett, and G. Wanner, *Solving ordinary differential equations I: Nonstiff problems*. Springer, 1993.

[171] C. Franke and R. Schaback, “Solving partial differential equations by collocation using radial basis functions,” *Applied Mathematics and Computation*, vol. 93, no. 1, pp. 73–82, 1998.

[172] Y. S. Cho and B. Joseph, “Reduced-order steady-state and dynamic models for separation processes. Part II. Application to nonlinear multicomponent systems,” *AICHE Journal*, vol. 29, no. 2, pp. 270–276, 1983.

[173] W. E. Stewart, K. L. Levien, and M. Morari, “Simulation of fractionation by orthogonal collocation,” *Chemical Engineering Science*, vol. 40, no. 3, pp. 409–421, 1985.

[174] C. L. E. Swartz and W. E. Stewart, “A collocation approach to distillation column design,” *AICHE Journal*, vol. 32, no. 11, pp. 1832–1838, 1986.

[175] G. M. Howard, “Unsteady state behavior of multicomponent distillation columns: Part I: Simulation,” *AICHE Journal*, vol. 16, no. 6, pp. 1022–1029, 1970.

[176] Z. Abdullah, N. Aziz, and Z. Ahmad, “Nonlinear Modelling Application in Distillation Column,” *Chemical Product and Process Modeling*, vol. 2, no. 3, 2007.

[177] J. C. Schulze, A. Caspari, C. Offermanns, A. Mhamdi, and A. Mitsos, “Nonlinear model predictive control of ultra-high-purity air separation units using transient wave propagation model,” *Computers & Chemical Engineering*, vol. 145, p. 107163, 2021.

[178] E. D. Gilles and B. Retzbach, “Reduced models and control of distillation columns with sharp temperature profiles,” in *1980 19th IEEE Conference on Decision and Control including the Symposium on Adaptive Processes*, pp. 865–870, 1980.

[179] Y. Cao, C. L. E. Swartz, J. Flores-Cerrillo, and J. Ma, “Dynamic modeling and collocation-based model reduction of cryogenic air separation units,” *AICHE Journal*, vol. 62, no. 5, pp. 1602–1615, 2016.

[180] Z. W. Huang, Y. M. Xu, C. Z. Fang, and J. Tang, “Improvements in dynamic compartmental modelling of distillation columns,” *Journal of Process Control*, vol. 3, no. 3, pp. 139–145, 1993.

[181] R. S. Kamath, I. E. Grossmann, and L. T. Biegler, “Aggregate models based on improved group methods for simulation and optimization of distillation systems,” *Computers & Chemical Engineering*, vol. 34, no. 8, pp. 1312–1319, 2010.

[182] A.-M. Ecker, I. Thomas, M. Häfele, B. Wunderlich, A. Obermeier, J. Ferstl, H. Klein, and A. Peschel, “Development of a new column shortcut model and its application in process optimisation,” *Chemical Engineering Science*, vol. 196, pp. 538–551, 2019.

[183] P. Schäfer, A. Caspari, K. Kleinhans, A. Mhamdi, and A. Mitsos, “Reduced dynamic modeling approach for rectification columns based on compartmentalization and artificial neural networks,” *AICHE Journal*, vol. 65, no. 5, p. e16568, 2019.

[184] W. Marquardt, “Nonlinear model reduction for binary distillation,” *Dynamics and Control of Chemical Reactors and Distillation Columns*, pp. 123–128, 1986.

[185] Y.-L. Hwang and F. G. Helfferich, “Nonlinear waves and asymmetric dynamics of countercurrent separation processes,” *AICHE Journal*, vol. 35, no. 4, pp. 690–693, 1989.

[186] A. Kienle, “Low-order dynamic models for ideal multicomponent distillation processes using nonlinear wave propagation theory,” *Chemical Engineering Science*, vol. 55, no. 10, pp. 1817–1828, 2000.

[187] A. Caspari, C. Offermanns, A. M. Ecker, M. Pottmann, G. Zapp, A. Mhamdi, and A. Mitsos, “A Wave Propagation Approach for Reduced Dynamic Modeling of Distillation Columns: Optimization and Control,” *Journal of Process Control*, vol. 91, pp. 12–24, 2020.

[188] A. Linhart and S. Skogestad, “Computational performance of aggregated distillation models,” *Computers & Chemical Engineering*, vol. 33, no. 1, pp. 296–308, 2009.

[189] J. D. Hedengren and T. F. Edgar, “Order Reduction of DAE Models,” *IFAC Proceedings Volumes*, vol. 38, no. 1, pp. 106–111, 2005.

[190] A. Kumar and P. Daoutidis, “Nonlinear model reduction and control for high-purity distillation columns,” *Industrial & engineering chemistry research*, vol. 42, no. 20, pp. 4495–4505, 2003.

[191] X. Qian, Q. Dang, S. Jia, Y. Yuan, K. Huang, H. Chen, and L. Zhang, “Operation of distillation columns using model predictive control based on dynamic mode decomposition method,” *Industrial & engineering chemistry research*, vol. 62, no. 50, pp. 21721–21739, 2023.

[192] M. Picon-Nunez, G. T. Polley, and M. Medina-Flores, “Thermal design of multi-stream heat exchangers,” *Applied Thermal Engineering*, vol. 22, no. 14, pp. 1643–1660, 2002.

[193] R. K. Shah and D. P. Sekulic, *Fundamentals of heat exchanger design*. John Wiley & Sons, 2003.

[194] X. Luo, M. Li, and W. Roetzel, “A general solution for one-dimensional multistream heat exchangers and their networks,” *International Journal of Heat and Mass Transfer*, vol. 45, no. 13, pp. 2695–2705, 2002.

[195] Xia, Abreu-Garcia, and Hartley, “Modelling and simulation of a heat exchanger,” in *IEEE International Conference on Systems Engineering*, pp. 453–456, IEEE, 1991.

[196] M. Baldea and P. Daoutidis, “Model reduction and control of reactor–heat exchanger networks,” *Journal of Process Control*, vol. 16, no. 3, pp. 265–274, 2006.

[197] B. Xu, A. Yebi, M. Hoffman, and S. Onori, “A rigorous model order reduction framework for waste heat recovery systems based on proper orthogonal decomposition and galerkin projection,” *IEEE Transactions on Control Systems Technology*, vol. 28, no. 2, pp. 635–643, 2018.

[198] P. Christ and T. Sattelmayer, “Reduced order modelling of flow and mixing in an automobile HVAC system using proper orthogonal decomposition,” *Applied Thermal Engineering*, vol. 133, pp. 211–223, 2018.

[199] J. Ma, D. Kim, and J. E. Braun, “Proper orthogonal decomposition for reduced order dynamic modeling of vapor compression systems,” *International Journal of Refrigeration*, vol. 132, pp. 145–155, 2021.

[200] Y. Xu, M. Peng, A. Cammi, C. Introini, and G. Xia, “Model order reduction of a once-through steam generator via dynamic mode decomposition,” *Annals of Nuclear Energy*, vol. 201, p. 110457, 2024.

[201] X. Li, Q. Xu, S. Wang, K. Luo, and J. Fan, “A novel data-driven reduced-order model for the fast prediction of gas-solid heat transfer in fluidized beds,” *Applied Thermal Engineering*, vol. 253, p. 123670, 2024.

[202] K. W. Hansen and K. Demandt, “Dynamics of a cross-flow heat exchanger with fins,” *International Journal of Heat and Mass Transfer*, vol. 17, no. 9, pp. 1029–1036, 1974.

[203] A. W. K. Quarshie, C. L. E. Swartz, P. B. Madabhushi, Y. Cao, Y. Wang, and J. Flores-Cerrillo, “Modeling, simulation, and optimization of multiproduct cryogenic air separation unit startup,” *AIChE Journal*, vol. 69, no. 2, 2023.

[204] K. W. Mathisen, M. Morari, and S. Skogestad, “Dynamic models for heat exchangers and heat exchanger networks,” *Computers & Chemical Engineering*, vol. 18, pp. S459–S463, 1994.

[205] A. Zavala-Rio and R. Santiesteban-Cos, “Reliable compartmental models for double-pipe heat exchangers: An analytical study,” *Applied Mathematical Modelling*, vol. 31, no. 9, pp. 1739–1752, 2007.

[206] A. Michel and A. Kugi, “Accurate low-order dynamic model of a compact plate heat exchanger,” *International Journal of Heat and Mass Transfer*, vol. 61, pp. 323–331, 2013.

[207] J. M. Jensen and H. Tummescheit, “Moving boundary models for dynamic simulations of two-phase flows,” *Proceedings of the 2nd international modelica conference*, pp. 235–244, 2002.

[208] Y. Vaupel, W. R. Huster, F. Holtorf, A. Mhamdi, and A. Mitsos, “Analysis and improvement of dynamic heat exchanger models for nominal and start-up operation,” *Energy*, vol. 169, pp. 1191–1201, 2019.

[209] A. Linhart and S. Skogestad, “An aggregation model reduction method for one-dimensional distributed systems,” *AIChE Journal*, vol. 58, no. 5, pp. 1524–1537, 2012.

[210] T. F. Yee, I. E. Grossmann, and Z. Kravanja, “Simultaneous optimization models for heat integration—I. Area and energy targeting and modeling of multi-stream exchangers,” *Computers & Chemical Engineering*, vol. 14, no. 10, pp. 1151–1164, 1990.

[211] M. M. F. Hasan, I. A. Karimi, H. E. Alfadala, and H. Grootjans, “Operational modeling of multistream heat exchangers with phase changes,” *AIChE Journal*, vol. 55, no. 1, pp. 150–171, 2009.

[212] U. Maas and S. B. Pope, “Simplifying chemical kinetics: Intrinsic low-dimensional manifolds in composition space,” *Combustion and Flame*, vol. 88, no. 3-4, pp. 239–264, 1992.

[213] D. G. Vlachos, “Reduction of detailed kinetic mechanisms for ignition and extinction of premixed hydrogen/air flames,” *Chemical Engineering Science*, vol. 51, no. 16, pp. 3979–3993, 1996.

[214] B. J. Reizman and K. F. Jensen, “An Automated Continuous-Flow Platform for the Estimation of Multistep Reaction Kinetics,” *Organic Process Research & Development*, vol. 16, no. 11, pp. 1770–1782, 2012.

[215] K. A. Hoo and D. Zheng, “Low-order control-relevant models for a class of distributed parameter systems,” *Chemical Engineering Science*, vol. 56, no. 23, pp. 6683–6710, 2001.

[216] N. Vora and P. Daoutidis, “Nonlinear model reduction of chemical reaction systems,” *AIChE Journal*, vol. 47, no. 10, pp. 2320–2332, 2001.

[217] S. H. Lam and D. A. Goussis, “The CSP method for simplifying kinetics,” *International journal of chemical kinetics*, vol. 26, no. 4, pp. 461–486, 1994.

[218] A. N. Gorban, I. V. Karlin, and A. Y. Zinovyev, “Invariant grids for reaction kinetics,” *Physica A: Statistical Mechanics and its Applications*, vol. 333, pp. 106–154, 2004.

[219] T. Lu and C. K. Law, “A directed relation graph method for mechanism reduction,” *Proceedings of the Combustion Institute*, vol. 30, no. 1, pp. 1333–1341, 2005.

[220] P. Pepiot-Desjardins and H. Pitsch, “An efficient error-propagation-based reduction method for large chemical kinetic mechanisms,” *Combustion and Flame*, vol. 154, no. 1-2, pp. 67–81, 2008.

[221] K. Edwards, T. F. Edgar, and V. I. Manousiouthakis, “Kinetic model reduction using genetic algorithms,” *Computers & Chemical Engineering*, vol. 22, no. 1-2, pp. 239–246, 1998.

[222] L. Petzold and W. Zhu, “Model reduction for chemical kinetics: An optimization approach,” *AIChE Journal*, vol. 45, no. 4, pp. 869–886, 1999.

[223] B. Bhattacharjee, D. A. Schwer, P. I. Barton, and W. H. Green, “Optimally-reduced kinetic models: reaction elimination in large-scale kinetic mechanisms,” *Combustion and Flame*, vol. 135, no. 3, pp. 191–208, 2003.

[224] A. N. Gorban and I. V. Karlin, “Method of invariant manifold for chemical kinetics,” *Chemical Engineering Science*, vol. 58, no. 21, pp. 4751–4768, 2003.

[225] E. Chiavazzo, A. N. Gorban, and I. V. Karlin, “Comparison of invariant manifolds for model reduction in chemical kinetics,” *Commun. Comput. Phys.*, vol. 2, no. 5, pp. 964–992, 2007.

[226] T. J. Snowden, P. H. van der Graaf, and M. J. Tindall, “Methods of model reduction for large-scale biological systems: a survey of current methods and trends,” *Bulletin of mathematical biology*, vol. 79, pp. 1449–1486, 2017.

[227] W. Ji, W. Qiu, Z. Shi, S. Pan, and S. Deng, “Stiff-PINN: Physics-Informed Neural Network for Stiff Chemical Kinetics,” *The journal of physical chemistry. A*, vol. 125, no. 36, pp. 8098–8106, 2021.

[228] M. Wen, E. W. C. Spotte-Smith, S. M. Blau, M. J. McDermott, A. S. Krishnapriyan, and K. A. Persson, “Chemical reaction networks and opportunities for machine learning,” *Nature computational science*, vol. 3, no. 1, pp. 12–24, 2023.

[229] S. Kasiraju and D. G. Vlachos, “LearnCK: mass conserving neural network reduction of chemistry and species of microkinetic models,” *Reaction Chemistry & Engineering*, vol. 9, no. 1, pp. 119–131, 2023.

[230] J. Pateras, C. Zhang, S. Majumdar, A. Pal, and P. Ghosh, “Physics-informed machine learning for automatic model reduction in chemical reaction networks,” *Scientific Reports*, vol. 15, no. 1, p. 7980, 2025.

[231] H. M. Park and D. H. Cho, “Low dimensional modeling of flow reactors,” *International Journal of Heat and Mass Transfer*, vol. 39, no. 16, pp. 3311–3323, 1996.

[232] K. Krischer, R. Rico-Martinez, I. G. Kevrekidis, H. H. Rotermund, G. Ertl, and J. L. Hudson, “Model identification of a spatiotemporally varying catalytic reaction,” *AIChE Journal*, vol. 39, no. 1, pp. 89–98, 1993.

[233] A. Armaou and P. D. Christofides, “Dynamic optimization of dissipative PDE systems using nonlinear order reduction,” *Chemical Engineering Science*, vol. 57, no. 24, pp. 5083–5114, 2002.

[234] C. Foias, M. S. Jolly, I. G. Kevrekidis, G. R. Sell, and E. S. Titi, “On the computation of inertial manifolds,” *Physics Letters A*, vol. 131, no. 7-8, pp. 433–436, 1988.

- [235] K. W. Hansen, “Analysis of transient models for catalytic tubular reactors by orthogonal collocation,” *Chemical Engineering Science*, vol. 26, no. 10, pp. 1555–1569, 1971.
- [236] L. Lefèvre, D. Dochain, S. Feyo de Azevedo, and A. Magnus, “Optimal selection of orthogonal polynomials applied to the integration of chemical reactor equations by collocation methods,” *Computers & Chemical Engineering*, vol. 24, no. 12, pp. 2571–2588, 2000.
- [237] J. Haag, C. Gentric, C. Lemaitre, and J.-P. Leclerc, “Modelling of Chemical Reactors: From Systemic Approach to Compartmental Modelling,” *International Journal of Chemical Reactor Engineering*, vol. 16, no. 8, 2018.
- [238] P. D. Christofides and P. Daoutidis, “Feedback control of two-time-scale nonlinear systems,” *International journal of control*, vol. 63, no. 5, pp. 965–994, 1996.
- [239] A. Kumar and P. Daoutidis, “Nonlinear dynamics and control of process systems with recycle,” *Journal of Process Control*, vol. 12, no. 4, pp. 475–484, 2002.
- [240] A. Caspari, C. Tsay, A. Mhamdi, M. Baldea, and A. Mitsos, “The integration of scheduling and control: Top-down vs. bottom-up,” *Journal of Process Control*, vol. 91, pp. 50–62, 2020.
- [241] S. Engell and I. Harjunkoski, “Optimal operation: Scheduling, advanced control and their integration,” *Computers & Chemical Engineering*, vol. 47, pp. 121–133, 2012.
- [242] L. Petzold, “Differential/algebraic equations are not ODE’s,” *SIAM Journal on Scientific and Statistical Computing*, vol. 3, no. 3, pp. 367–384, 1982.
- [243] M. Morari and U. Maeder, “Nonlinear offset-free model predictive control,” *Automatica*, vol. 48, no. 9, pp. 2059–2067, 2012.
- [244] G. E. Karniadakis, I. G. Kevrekidis, L. Lu, P. Perdikaris, S. Wang, and L. Yang, “Physics-informed machine learning,” *Nature Reviews Physics*, vol. 3, no. 6, pp. 422–440, 2021.
- [245] A. Gouasmi, E. J. Parish, and K. Duraisamy, “A priori estimation of memory effects in reduced-order models of nonlinear systems using the Mori-Zwanzig formalism,” *Proceedings of the Royal Society A*, vol. 473, no. 2205, p. 20170385, 2017.
- [246] S. E. Ahmed, S. Pawar, O. San, A. Rasheed, T. Iliescu, and B. R. Noack, “On closures for reduced order models—A spectrum of first-principle to machine-learned avenues,” *Physics of Fluids*, vol. 33, no. 9, p. 091301, 2021.
- [247] W. M. Czarnecki, S. Osindero, M. Jaderberg, G. Swirszcz, and R. Pascanu, “Sobolev training for neural networks,” *Advances in Neural Information Processing Systems*, vol. 30, 2017.
- [248] C. Tsay, “Sobolev trained neural network surrogate models for optimization,” *Computers & Chemical Engineering*, vol. 153, p. 107419, 2021.
- [249] N. K. Yamaleev and K. A. Pathak, “Nonlinear model reduction for unsteady discontinuous flows,” *Journal of Computational Physics*, vol. 245, pp. 1–13, 2013.
- [250] L. Bettini, M. Cenedese, and G. Haller, “Model reduction to spectral submanifolds in piecewise smooth dynamical systems,” *International Journal of Non-Linear Mechanics*, vol. 163, p. 104753, 2024.